

California Deepwater Investigations and Groundtruthing (Cal DIG) I, Volume 2: Fault and Shallow Geohazard Analysis Offshore Morro Bay



California Deepwater Investigations and Groundtruthing (Cal DIG) I, Volume 2: Fault and Shallow Geohazard Analysis Offshore Morro Bay

November 2021

Authors:

M.A.L Walton¹, C.K. Paull², G. Cochrane¹, J. Addison³, D. Caress², R. Gwiazda², D. Kennedy¹, E. Lundsten², A. Papesh¹

¹U.S. Geological Survey Pacific Coastal and Marine Science Center, Santa Cruz, CA

²Monterey Bay Aquarium Research Institute (MBARI), Moss Landing, CA

³U.S. Geological Survey Geology, Minerals, Energy, and Geophysics Science Center, Moffett Field, CA

Prepared under BOEM-USGS Intra-Agency Agreement Number M17PG00021

By

U.S. Geological Survey
Pacific Coastal and Marine Science Center
2885 Mission Street
Santa Cruz, CA 95060

US Department of the Interior
Bureau of Ocean Energy Management
Pacific OCS Region



DISCLAIMER

This study was funded, in part, by the U.S. Department of the Interior, Bureau of Ocean Energy Management (BOEM), Environmental Studies Program, Washington, DC, through Intra-Agency Agreement Number M17PG00021 with the U.S. Geological Survey. This report has been technically reviewed by BOEM, and it has been approved for publication. The views and conclusions contained in this document are those of the authors and should not be interpreted as representing the opinions or policies of BOEM. This document has been peer reviewed and approved for publication consistent with USGS Fundamental Science Practices (<https://pubs.usgs.gov/circ/1367/>). Any use of trade, firm, or product names is for descriptive purposes only and does not imply endorsement by the U.S. Government.

REPORT AVAILABILITY

To download a PDF file of this report, go to the U.S. Department of the Interior, Bureau of Ocean Energy Management [Data and Information Systems webpage](http://www.boem.gov/Environmental-Studies-EnvData/) (<http://www.boem.gov/Environmental-Studies-EnvData/>), click on the link for the Environmental Studies Program Information System (ESPIS), and search on 2021-044.

CITATION

Walton MAL, Paull CK, Cochrane G, Addison J, Caress D, Gwiazda R, Kennedy D, Lundsten E, Papesh A. 2021. California Deepwater Investigations and Groundtruthing (Cal DIG) I, Volume 2: Fault and Shallow Geohazard Analysis Offshore Morro Bay. Camarillo (CA): U.S. Department of the Interior, Bureau of Ocean Energy Management. OCS Study BOEM 2021-044. 56 p.

ABOUT THE COVER

The NOAA Ship *Rainier* in port in San Francisco in August 2018 prior to data collection for this study. Photo credit: Maureen Walton, USGS.

ACKNOWLEDGMENTS

Big thanks to Lisa Gilbane, Jared Kluesner, Linda Kuhnz, Jen Miller, Ray Sliter, Tom Lorenson, Mary McGann, the USGS marine technicians, and the crews of the R/V *Bold Horizon*, the NOAA Ship *Rainier*, the R/V *Rachel Carson*, and the R/V *Western Flyer* for their vital support during data collection and processing, and for helpful scientific discussions. Additional thanks to Lisa Gilbane, Gary Greene, Jared Kluesner, Jen Miller, Robbie Dame, Steve Dobbs, Sam Johnson, Tom Lorenson, and Mike Rasser for their feedback, reviews, and contributions to the text and figures in this report.

Contents

List of Figures	ii
List of Tables.....	iii
List of Abbreviations and Acronyms.....	iv
Executive Summary	v
1 Introduction	1
2 Methods	2
2.1 Geophysical reconnaissance surveys	3
2.1.1 NOAA Ship <i>Rainier</i> , August through September 2018.....	3
2.1.2 R/V <i>Rachel Carson</i> , April 2018, March and May 2019.....	4
2.2 Groundtruthing and sampling surveys.....	4
2.2.1 R/V <i>Bold Horizon</i> , September 2019	4
2.2.2 R/V <i>Western Flyer</i> , February 2019 and November 2019	5
2.3 Multibeam echosounder data	5
2.4 Integrative data interpretation	6
3 Results	9
3.1 Subsurface stratigraphy.....	9
3.2 Fault structure and scarps mapping	11
3.3 Pockmark mapping	12
3.4 Preliminary results from core analysis	12
4 Discussion.....	13
4.1 Fault hazards	13
4.2 Pockmark hazards	15
4.3 Sediment gravity flows hazards	16
5 Conclusions	16
6 References.....	45

List of Figures

Figure 1. Region of study offshore of Morro Bay, central California.	18
Figure 2. Map of geophysical data.	19
Figure 3. Map of sampling data.	20
Figure 4. Maps of gridded subsurface horizons in the pockmark area (1 of 2).	21
Figure 5. Maps of gridded subsurface horizons in the pockmark area (2 of 2).	22
Figure 6. MCS and Chirp images showing subsurface mapping in the pockmark area.	23
Figure 7. Maps of gridded subsurface horizons in the basin area.	24
Figure 8. MCS image showing subsurface mapping in the basin area.	25
Figure 9. Maps of gridded subsurface horizons in the SLB north area.	26
Figure 10. MCS image showing subsurface mapping in the SLB north area.	27
Figure 11. Maps of gridded subsurface horizons in the SLB south area (1 of 2).	28
Figure 12. Maps of gridded subsurface horizons in the SLB south area (2 of 2).	29
Figure 13. MCS image showing subsurface mapping in the SLB south area.	30
Figure 14. Maps of regional gridded subsurface horizons across several physiographic regions.	31
Figure 15. Sediment thickness map.	32
Figure 16. Map of fault structures in the study area.	33
Figure 17. MCS image crossing the Santa Lucia Bank fault.	34
Figure 18. AUV data along SLB scarps.	35
Figure 19. Mapped evidence for mass wasting.	36
Figure 20. Mapped evidence for pockmarks.	37
Figure 21. AUV data in the pockmark area.	38
Figure 22. Example piston core photographs from a pockmark core.	39
Figure 23. Example CT scan composite plot of a piston core in the pockmark region.	40
Figure 24. Plot of porewater and MSCL data from pockmark piston cores.	41
Figure 25. Plot of porewater and MSCL data from the Lucia Chica channel area.	42
Figure 26. Plot of porewater and MSCL data from piston cores located downslope and east of SLB.	43
Figure 27. Example vibracore photographs from a transect along an SLB fault.	44

List of Tables

Table 1. <i>R/V Bold Horizon</i> core processing status by core as of 18 June 2021.	8
--	---

List of Abbreviations and Acronyms

AUV	Autonomous underwater vehicle
BOEM	Bureau of Ocean Energy Management
BP	Before present
Cal DIG	California Deepwater Investigations and Groundtruthing
Chirp	Compressed high intensity radar pulse
CT	Computerized tomography
DOI	US Department of the Interior
ESP	Environmental Studies Program
ESPIS	Environmental Studies Program Information System
GC	Gravity core
Hz	Hertz
JPC	Jumbo piston core
LCC	Lucia Chica channel
MBARI	Monterey Bay Aquarium Research Institute
MBES	Multibeam echosounder
MBNMS	Monterey Bay National Marine Sanctuary
MCS	Multi-channel seismic
MSCL	Multi-sensor core logger
MTD	Mass-transport deposit
Myr	Million years
NOAA	National Oceanic and Atmospheric Administration
OCS	Outer continental shelf
Pre-Q	Pre-Quaternary
Q	Quaternary
QFO	Quaternary Faults Offshore
ROV	Remotely operated vehicle
R/V	Research Vessel
SGHF	San Gregorio-Hosgri fault
SLB	Santa Lucia Bank
SLBF	Santa Lucia Bank fault
SSC	San Simeon channel
SU	Seismic Unix
TWTT	Two-way travel time
USGS	U.S. Geological Survey
VC	Vibracore

Executive Summary

The California Deepwater Investigations and Groundtruthing (Cal DIG) I project focuses on the potential seafloor hazards and impacts of alternative energy infrastructure in the outer continental shelf region offshore of south-central California. This is one of three reports covering a single study area located between Monterey and Point Conception, California, in Federal waters outside of the State of California three nautical mile limit and in water depths of 400 to 1500 meters. The goal of this report is to provide baseline geologic interpretations of the area for the purpose of improving regional models of shallow geologic hazards and sedimentary processes. Geophysical and geological data from this project will help to address important issues associated with marine spatial planning and potential offshore infrastructure development, such as offshore floating wind turbines. Datasets covered in this report include comprehensive high-resolution sub-bottom (multi-channel and Chirp seismic reflection profiles), seafloor (bathymetry), and sampling (piston, gravity, and vibracore) data collected in 2018–2019, during a series of seven seagoing geological and geophysical surveys. Specifically, this report outlines interpretation of subsurface geologic structure from the geophysical data, details preliminary core analysis results related to fluid, gas, and sediment transport activity, provides interpretations of the current geohazards in the area, and suggests next steps for improving interpretations of geohazard processes.

Specific targets of geohazard interest in the study area are geological structures such as faults and folds, seafloor pockmarks within a large field (the Big Sur pockmark field), submarine channels, and mass wasting (slope failure) features. The vast majority of faults and other structures in the study occur within sediment and rock formations we interpret to be pre-Quaternary (older than 2.58 Myr BP), and thus we interpret that these structures are unlikely to present substantial current hazard to seabed infrastructure, although we note that the numerous structures mapped in the study area may have the potential to become reactivated. Similarly, we find no new evidence of Holocene (younger than 11,650 years BP) fluid or gas advection in the Big Sur pockmark field. However, such fluid and gas hazards are currently difficult to assess, as additional analyses and sampling of existing core data is needed to better understand pockmark formation processes and potential gas accumulations we have mapped in the subsurface. Mass wasting along the eastern and western edges of the Santa Lucia Bank during earthquakes, as well as sediment transport down the Lucia Chica and San Simeon channels, are among the most noteworthy, although still likely infrequent during the Holocene, hazards to seabed stability in the study area. Further analyses of the existing cores, including radiocarbon dating, stable isotope analysis, and compositional analysis, are again needed to better understand the timing and sources of the numerous sand deposits found throughout the study area, which may have been transported downslope due to mass wasting and/or earthquake shaking processes.

1 Introduction

The potential direct, indirect, and cumulative impacts on the human, coastal, and marine environments must be evaluated before the Bureau of Ocean Energy Management (BOEM) can make environmentally sound decisions for managing energy activities and developing mitigation measures to avoid or minimize impacts. Potential offshore energy developers have indicated interest in areas farther offshore of the continental shelf due to higher resource potential and to minimize fishing conflicts. Because of this interest, the State of California has actively engaged BOEM to identify sites for offshore energy projects within the outer continental shelf (OCS), in Federal waters outside of the State of California three nautical mile limit. In 2018, BOEM issued a public call for interest and information for three defined areas of the California OCS (two areas shown in Fig. 1). These OCS areas cover the seafloor over many kilometers in an active tectonic region adjacent to the Pacific-North American Plate boundary, and thus BOEM has a critical need for data that address shallow fault activity, seafloor morphology, and site characterization. These data are critical for understanding risks to proposed energy projects and useful for mitigation of environmental impacts to sensitive seafloor habitats. Geophysical and geological data acquisition and interpretation methods reported herein provide baseline maps of the seafloor physiography needed to assess viability of proposed offshore development.

The geographic scope of the California Deepwater Investigations and Groundtruthing (Cal DIG) I project focuses on offshore Morro Bay in the south-central OCS of California in water depths ranging from 400 to 1500 meters (Fig. 1). This specific region is of interest for offshore wind energy development due to its proximity to power grid infrastructure south of Morro Bay, California (e.g., the Diablo Canyon Power Plant), and consistently high offshore wind speeds. Geophysical and geological data from this project will help to address important issues associated with marine spatial planning, ecosystem assessments (e.g., benthic habitats), geologic hazards, sediment transport, offshore infrastructure siting, and offshore infrastructure development. Although previous geophysical and geologic mapping has been conducted by various academic, government, and private agencies in a number of Pacific OCS areas, this study provides comprehensive high-resolution sub-bottom, seafloor, and sampling data in the south-central California OCS for the first time.

For this investigation, herein we address several scientific topics that focus on geologic hazards processes, specifically those associated with earthquakes, tsunamis, submarine landslides, sediment transport, mass wasting, and fluid and gas advection, all of which occur in the study area. For example, there is some evidence for recent, noteworthy seismicity along local faults, including the 1927 Lompoc, California, M7.0 earthquake, which may have occurred along the nearby Hosgri transform fault (Gawthrop, 1978; Fig. 1). Tsunami models suggest that the Lompoc earthquake may actually have occurred closer to the Santa Lucia Bank (SLB) (Helmlberger et al., 1992; Satake and Somerville, 1992), which lies in the southern part of our study area. While most of SLB is largely devoid of recorded recent seismicity (Fig. 1), two thrust events (M5.8 and M6.0) occurred in 1969 southwest of SLB (Gawthrop, 1975; Fig. 1). Previous work related to fault and earthquake activity has been focused on understanding regional-scale deformation resulting from Cretaceous subduction along the margin (McCulloch et al., 1980, 1982; McCulloch, 1987; Namson and Davis, 1990) as well as the tectonics of the San Gregorio-Hosgri fault system (Dickinson et al., 2005; Johnson et al., 2018). Little has been published on mass wasting processes, and sediment transport research in the study area has focused on turbidity flow activity in the Lucia Chica channel (Maier et al., 2011, 2012, 2013). The ~1300 km² Big Sur pockmark field in the northern region of the study area may be linked to rapid release of methane gas at the seafloor and may record a history of fluid advection in the subsurface, although previous work shows no evidence of these processes in the Holocene (since 11,650 years BP; Paull et al., 2002).

The objectives of this study are to examine Quaternary fault structure and evidence for fault motion and past earthquakes that may be recorded by fault deformation and in basin sediments, including seismically triggered mass wasting (e.g., Normark and Gutmacher, 1988; Goldfinger et al., 2012). We also re-examine the physical characteristics in the pockmark field toward determining recency of fluid and gas advection, and identify past turbidity flows within two major submarine channel systems traversing our study area, the Lucia Chica and San Simeon channels (Fig. 1). The U.S. Geological Survey (USGS), in partnership with BOEM, the Monterey Bay Aquarium Research Institute (MBARI), and the National Oceanic and Atmospheric Administration (NOAA), conducted high-resolution geophysical and geological surveys in 2018 and 2019 that allow for a comprehensive analysis of the seafloor and shallow subsurface geology that we use to interpret sedimentary turbidity flows, fault activity, and active fluid flow (Figs. 2 and 3). Methods presented here include the interpretation of high-resolution multichannel seismic (MCS) reflection and Chirp sub-bottom profile data in conjunction with surface-ship multibeam echosounder (MBES) and autonomous underwater vehicle (AUV) seafloor bathymetric data. We also present preliminary analysis of seabed piston, gravity, and vibracore data collected by the USGS and MBARI in the study area during the same time period.

Our results show little-to-no evidence of fault activity within Quaternary (within the past 2.58 Myr) stratigraphy, but abundant evidence for faults and folds within pre-Quaternary stratigraphy exposed at the seafloor, especially in the SLB area. We have no new evidence of Holocene (since 11,650 years BP) fluid or gas advection in the Big Sur pockmark field, but we find some seismic evidence of geologic events beneath pockmarks, as well as gas (perhaps methane) accumulation in the subsurface just east of the pockmark field; however, our results thus far are inconclusive about pockmark formation processes and the timing of earlier activity. Lastly, preliminary analysis of core data shows abundant evidence for Quaternary turbidity flows and slope failures in the channels and along the edges of SLB, some of which may have been triggered by earthquakes on the nearby Hosgri-San Gregorio fault system. Future work will include continued analysis of the core data in conjunction with the geophysical data, as well as collection of core samples for ^{14}C dating and other analyses (e.g., composition, stable isotopes, grain size) to better constrain the nature and timing of pockmark events and sediment transport in the study area.

2 Methods

A combination of surface-ship, targeted AUV, piston and gravity coring, and remotely operated vehicle (ROV) surveys were conducted during seven cruises that took place in 2018–2019 in the study region to meet study objectives. First, in August–September 2018, an initial surface-ship geophysical reconnaissance survey was conducted aboard the NOAA Ship *Rainier*. In 2019, three AUV high-resolution geophysical reconnaissance surveys were conducted aboard the MBARI R/V *Rachel Carson*. Early in February 2019, the first of three groundtruthing surveys was conducted aboard MBARI R/V *Western Flyer* to collect ROV video, push-core, rock sample, and vibracore data. In late 2019, after data from the surface-ship and AUV geophysical surveys were processed, two final groundtruthing surveys were conducted. In September 2019, the R/V *Bold Horizon* collected piston cores, gravity cores, and ROV video data, and in November 2019, the MBARI R/V *Western Flyer* again collected ROV video data, push-cores, rock samples, and vibracores. Below we outline the data collection, processing, and interpretation methods, and provide links to relevant data releases and data downloads.

2.1 Geophysical reconnaissance surveys

2.1.1 NOAA Ship *Rainier*, August through September 2018

The initial geophysical surface-ship site survey for the project was conducted over two legs, totaling 22 days at sea aboard the NOAA Ship *Rainier* (USGS cruise ID 2018-641-FA), with mobilization for the survey beginning on 24 August 2018 and demobilization ending on 21 September 2018. There was a 2-day port call in Long Beach, California, from 8–9 September 2018, during which time personnel transfers and refuel/resupply occurred. Data collection was primarily in the proposed Cal DIG I study area (Fig. 2) but also included ~36 hours of data collection in Santa Barbara Basin, our contingency weather area. MCS and Chirp data collected aboard the *Rainier* are available for public download via a USGS data release (Kennedy et al., 2021a).

2.1.1.1 MCS survey acquisition and processing parameters

While the NOAA Ship *Rainier* is primarily a hydrographic vessel (data collection detailed in Cochrane et al., 2021a, 2021b), during multibeam acquisition, the USGS simultaneously collected low-energy minisparker MCS data in the contour-parallel (strike line) pattern required for MBES acquisition using the hydrographic systems on the *Rainier* (Fig. 2). Sub-perpendicular, survey-crossing (dip line) MCS tracklines were run near the end of each leg to tie data together (Fig. 2). The USGS deployed a SIG 2-Mille minisparker system capable of operating at power levels between 300–1200 J; during our survey we collected data at reduced source energy levels of 700 J – 1 kJ, as per Categorical Exclusion environmental compliance requirements. The frequency range of the minisparker is ~100–1200 Hz. During our survey, the minisparker source was tied to a cleat and towed from the aft port side of the *Rainier*. Shot interval during the survey was variable, but generally 3–4 seconds, with a record length ~0.5 seconds longer than the shot interval and a survey speed of ~6 knots. The multi-channel hydrophone streamer was deployed through a large scupper on the aft starboard side of the *Rainier*. We utilized an 8-section, 64-channel Geometrics GeoEel solid digital hydrophone streamer with variable spacing. The four near sections each had 8 hydrophone groups spaced at 1.5625 m, and the far four sections each had 8 hydrophones spaced at 3.125 m for a total active streamer length of ~150 m. Early on in the survey, we ran into issues with one of the near short sections and ended up removing a short section, running the majority of the survey with 56 channels. We attempted using floats on the streamer, but also removed those early on due to shallow towing and wave noise.

MCS data were processed by USGS personnel to a brutestack at sea using a combination of SIOSEIS and Seismic Unix (SU) software packages, and later to a poststack time migration using Echos processing software. In post-processing, we noticed a ghost reflection that indicated a sagging streamer (likely due to a lack of floats), causing a geometry shorter than our original assumptions. Because of the sagging streamer, a careful geometry analysis was completed for each line to apply the correct channel offsets. After geometry calculation, data were sorted into common midpoint gathers and frequency filtered to remove low-frequency wave noise and 60 Hz electronic noise (although we were unable to identify an electronics grounding issue at sea). A combination tapered bandpass filter and automatic noise frequency suppression notch filter were applied. Next, traces were median filtered to remove amplitude spikes, deconvolved using a spike deconvolution, moved out using a simple one-dimensional velocity model, stacked, and migrated, with a water-bottom mute also applied. After processing, we were able to resolve acoustic penetration over 500 m into the subsurface in some cases, with a vertical resolution of up to ~1–2 m.

2.1.1.2 Chirp survey acquisition and processing parameters

During the Cal DIG MCS survey aboard the *Rainier*, we also used an Edgetech 512i Chirp towfish operated at a 1–6 kHz sweep and deployed it from the *Rainier*'s main A-frame. We collected Chirp data only during the final ~36 hours of Leg 1 (Fig. 2). We attempted to deploy the Chirp during Leg 2, but a rough sea-state prevented us from a successful deployment. During Leg 1, the Chirp data were collected along sub-perpendicular dip lines across previously surveyed areas to best image structural features, map regional stratigraphic units, and assess potential future coring sites (Fig. 2). These dip lines were generally run at a slower (~4 knots) survey speed to protect the Chirp equipment, and all Chirp lines were collected with coincident MCS and MBES data. We acquired Chirp data in water depths up to ~1200 m, and we were able to image as much as 30–50 m acoustic penetration into the subsurface.

Chirp data were first converted from native .jsf format to .segy envelope format. Some of the water column was cropped to enable processing of a shorter record length, and a water-bottom mute was also applied to remove sparker crosstalk noise. Towfish depth and swell corrections were applied, and the data were median filtered and trace balanced where necessary to correct and balance amplitude variations introduced by sparker crosstalk and the Edgetech software auto-gain during acquisition. Where instrument shutdowns occurred due to the presence of marine wildlife or instrument malfunctions, missing traces were filled by blank traces. Lastly, data were spliced together and renamed to match their corresponding MCS lines.

2.1.2 R/V *Rachel Carson*, April 2018, March and May 2019

Three AUV cruises were conducted aboard the MBARI R/V *Rachel Carson* from 25–28 April 2018, 14–19 March 2019, and 10–11 May 2019. These surveys targeted channels, pockmarks, and structural features in the Cal DIG study region. A total of 20 AUV dives between the three cruises were conducted (Fig. 2). The MBARI AUV carries a Reson 7125 400 kHz multibeam sonar system and an Edgetech 1–6 kHz Chirp sub-bottom profile system (e.g., Caress et al., 2008). The 20 AUV surveys provided coincident ultra-high-resolution multibeam bathymetry and low-altitude Chirp data (Fig. 2). During multibeam acquisition, Chirp data were collected along sub-parallel tracklines and tied together with wider-spaced crossing lines. All data were processed by MBARI technicians. AUV bathymetric data were generally gridded to ~1 m cell size, and Chirp sub-bottom profile data were altitude corrected. AUV bathymetry and Chirp data are available for public download via a USGS data release (Kennedy et al., 2021b).

2.2 Groundtruthing and sampling surveys

2.2.1 R/V *Bold Horizon*, September 2019

The primary groundtruthing study was conducted over 13 days at sea between 9–26 September 2019 aboard the R/V *Bold Horizon* (USGS cruise ID 2019-642-FA). In this report we detail the results of the piston and gravity coring survey, although we note that seafloor video used for benthic habitat assessment was also conducted during the *Bold Horizon* survey using the MBARI mini-ROV (survey details in Kuhnz et al., 2021). Piston and gravity coring were conducted for the most part during daylight hours at the request of the crew of the R/V *Bold Horizon*, with the piston coring rail system arranged on the fantail at a slight diagonal to allow for a 10 m barrel setup. Cores were collected on 12 of the 13 days at sea for a total of 40 cores (Fig. 3).

At-sea processing of cores included taking 5-cm-long whole-round samples 17 cm from the bottom of the cores in areas where shallow gas was suspected (i.e., pockmark areas). These 5-cm whole-round samples were squeezed for pore water and methane analysis (Reebugh, 1980). As none of the samples evolved

noticeable quantities of gas, no gas samples were preserved. After sectioning cores, other porewater samples were extracted from most cores using rhizons (Dickens et al., 2007) and refrigerated for shore-based analysis of sulfate and chloride concentrations by ion chromatography at MBARI. While at sea, the cores were stored cold in a refrigerator, and after the cruise were transported and stored at the USGS core laboratory in Santa Cruz, California, the same day as offloading from the ship's refrigerator in port at Alameda, California.

The laboratory core processing workflow started with a multi-sensor core logger (MSCL) system logging the uncut whole core to collect core depth, core width, density, p-wave velocity, and magnetic susceptibility data. Optional computerized tomography (CT) scanning of select whole-round sections follows MSCL logging, then splitting, photographing, and describing each section. Finally, sampling of the cores for ^{14}C dating, grain size, mineralogy, and other analyses can occur. All piston and gravity cores were logged using the MSCL, split, and photographed, and some priority cores were CT scanned, described, and sampled (see Table 1 for a summary of the processing status). The R/V *Bold Horizon* data are available at Kennedy et al. (2021c). This data release includes processed data and data presented in this report (MSCL, porewater data, core photographs, and select CT scans).

2.2.2 R/V *Western Flyer*, February 2019 and November 2019

In addition to the R/V *Bold Horizon* work, two additional complementary groundtruthing surveys were conducted aboard the MBARI R/V *Western Flyer* using the on-board ROV, the *Doc Ricketts*. These surveys were funded completely by MBARI and designed to collect seabed video and photographs, push-core samples, and vibracores in the previously surveyed AUV areas. The first of the two surveys occurred from 6–12 February 2019 (USGS cruise ID 2019-603-FA) and collected 310 total seafloor samples and vibracores (Fig. 3). The second cruise from 2–10 November 2019 (USGS cruise ID 2019-667-FA) collected 477 seafloor samples and vibracores (Fig. 3).

Processing of the seafloor sample data follows similar procedures as outlined above for the R/V *Bold Horizon* piston and gravity cores. At sea, porewater samples were collected from some vibracores using rhizons. Sulfate and chloride concentrations were measured by ion chromatography in a sea-going porewater measurement van. Shore-based lab processing of the vibracores includes MSCL logging, CT scanning, splitting, photographing, describing, and sampling for ^{14}C analysis. Push-core stratigraphy was in most cases described at sea and some push-cores were preserved for ^{210}Pb and foraminifera dating. In this report, we primarily use vibracore observations to supplement observations from the R/V *Bold Horizon* piston and gravity cores. All sample data from the 2019 R/V *Western Flyer* surveys have been archived at MBARI, and data supporting conclusions in this report are available in a data release (Kennedy et al., 2021d), which includes select vibracore data (core photographs).

2.3 Multibeam echosounder data

While not the focus of this report, we utilized surface-ship MBES data to supplement our observations of the subsurface and geology (e.g., Fig. 1). A key piece of the MBES data was collected coincident with the previously described MCS and Chirp data during the 2018 *Rainier* survey using a hull-mounted MBES system (Kongsberg EM710). Bathymetric, seafloor backscatter, and water column data were collected using this system. Throughout our results and interpretations presented here, we utilize a merged 25-m bathymetric grid produced by MBARI that includes the 2018 *Rainier* data along with other surface-ship MBES data collected in the region, including a 2016 R/V *Sally Ride* survey (cruise ID SR1604), two additional NOAA Ship *Rainier* and *Fairweather* surveys (OPR-L397-RA-17 and OPR-L31-FA-19), and 2016-2019 transit data from the R/V *Sikuliaq*, R/V *Revelle*, and R/V *Falkor*. More details are in the

companion report by Cochrane et al. (2021a) and the associated habitat data release (Cochrane et al., 2021b).

2.4 Integrative data interpretation

The bulk of the subsurface interpretations we present here were done using IHS Kingdom Suite seismic interpretation software. Map-based analysis was completed using ArcGIS Desktop software.

A large part of the analysis presented here includes mapping of regional seismic reflection *surfaces* (relationships in acoustic reflections interpreted to reflect geology) in the MCS data using Kingdom Suite. For ease of mapping, we generally separated interpretations into four physiographic regions (see Fig. 3): pockmarks, basin, SLB north, and SLB south, as well as a fifth category of regional interpretations that extend into multiple physiographic regions (e.g., the seafloor). After being mapped on 2D MCS data, the mapped picks were gridded using an inverse distance to power algorithm in Kingdom Suite with a cell size of 100 m and a gridding search radius of 1.5–2.5 km depending on the regional coverage of the subsurface mapping (generally 1.5 km for higher-coverage, more regional surfaces and 2.0 or 2.5 km for lower-coverage, localized surfaces). These search distances were based on the typical minimum spacing of the seismic reflection profiles (~1.5 km) as well as the spacing in the grid area. Some grids, especially the more regional grids, were clipped using a convex hull polygon to reduce edge effects. After we generated grids in Kingdom Suite, we exported the gridded point data for import and visualization in ArcGIS Desktop.

The sediment thickness grid we present represents the minimum sediment thickness in the region mapped using high-resolution MCS data. Thickness was calculated by subtracting a merged grid of *acoustic basement* (hereafter, *basement*) picks from the mapped seafloor. The basement represents the limit of subsurface acoustic penetration of our MCS system, which can generally penetrate through and image sedimentary layers but not consolidated bedrock. We map basement seismic reflections in each of the 4 primary physiographic regions of the study area (see Fig. 3; pockmarks, basin, SLB north, and SLB south). Basement surfaces sometimes extend into neighboring regions, where the geology and therefore acoustic penetration is different; the variable acoustic penetration leads to a different acoustic basement surface, causing overlapping basement interpretations in some areas. Because the term “basement” should describe only the deepest seismic reflections, it is not an accurate way to describe surfaces in areas where our basement interpretations overlap; thus, we use the broader term “deep” to describe those surfaces that include some picks of acoustic basement. To generate the sediment thickness map, we have merged together the most regionally expansive deep grids from each of the four primary physiographic regions to provide a minimum sediment thickness map. Any overlapping grid edges were blended using a horizontally weighted calculation of the values of the overlapping cells. All values were calculated using two-way travel time (TWTT) grids and are thus reported in TWTT as well. Assuming a seismic velocity of 2000 m/s, sediment thickness in TWTT can be loosely approximated as 1 ms = 1 m.

Fault analysis was completed both in Kingdom and in ArcGIS. Mapped subsurface fault segments from Kingdom Suite were categorized as Quaternary or pre-Quaternary based on whether they offset the seafloor and/or shallowest sedimentary packages (layers) in areas likely to have Quaternary sediment (basin, pockmarks, and some areas of SLB). Faults were further categorized as “tectonic” if they exhibit basement-involved vertical displacements, untraceable stratigraphy, substantial folding or deformation, and/or abrupt changes in lithology across the fault segments; tectonic faults exist for both Quaternary and pre-Quaternary segments. For visualization in map view, the surficial projections of the mapped subsurface fault segments were imported into ArcGIS as a point dataset. We also mapped linear scarps in ArcGIS by looking for steep slopes in bathymetric slope and elevation data and by considering the subsurface mapping; subsurface fault segment projections, particularly of tectonic and Quaternary faults,

assisted with mapping of scarp features in bathymetric data in some cases. Because few faults in the study area are continuous, Quaternary, or tectonic in nature, we present our maps of surficial fault mapping together with the subsurface fault segment projections for the most complete interpretive information about the fault structures in the study area.

Table 1. R/V *Bold Horizon* core processing status by core as of 18 June 2021.

Core processing is ongoing at the USGS core laboratory facility in Santa Cruz, California. JPC = jumbo piston core. GC = gravity core. MSCL = multi-sensor core logger. CT = computerized tomography.

Core ID	Latitude	Longitude	Analyses completed	Analysis needed
01JPC	34.535102	-121.106945	porewater, MSCL, split/photo, describe	sample
02JPC	34.866482	-121.198425	porewater, MSCL, split/photo, describe	sample
03JPC	35.025135	-121.270938	porewater, MSCL, split/photo, describe	sample
04JPC	34.952035	-121.392427	MSCL, split/photo	describe, sample
05GC	34.845972	-121.375367	MSCL, split/photo	describe, sample
06GC	35.056410	-121.324847	MSCL, split/photo	describe, sample
07JPC	35.077682	-121.300355	porewater, MSCL, split/photo	describe, sample
08GC	35.010445	-121.427798	(none – only a sample recovered at site)	sample
09GC	34.992700	-121.440062	MSCL, split/photo	describe, sample
10GC	35.048738	-121.552972	porewater, MSCL, split/photo	describe, sample
11JPC	35.514538	-121.628627	porewater, MSCL, split/photo	describe, sample
12JPC	35.522640	-121.642205	porewater, MSCL, split/photo	describe, sample
13JPC	35.516332	-121.630253	porewater, MSCL, split/photo	describe, sample
14JPC	35.474828	-121.470360	porewater, MSCL, split/photo, described, sampled	(none)
15GC	35.478435	-121.480868	MSCL, split/photo, described	sample
16GC	35.475780	-121.480893	porewater, MSCL, split/photo, described	sample
17JPC	35.496912	-121.486462	porewater, MSCL, split/photo, described	sample
18JPC	35.486510	-121.480078	porewater, MSCL, split/photo, described, sampled	(none)
19JPC	35.442555	-121.467845	porewater, MSCL, split/photo, described	sample
20JPC	35.293690	-121.443620	MSCL, split/photo	describe, sample
21JPC	35.211030	-121.404392	porewater, MSCL, split/photo	describe, sample
22JPC	35.211263	-121.400542	porewater, MSCL, split/photo	describe, sample
23JPC	35.605552	-121.604717	porewater, MSCL, CT, split/photo	describe, sample
24JPC	35.608663	-121.604933	porewater, MSCL, split/photo	describe, sample
25JPC	35.739467	-121.780582	MSCL, split/photo	describe, sample
26JPC	35.740147	-121.779737	MSCL, split/photo	describe, sample
27JPC	35.732340	-121.766913	porewater, MSCL, split/photo	describe, sample
28GC	35.734065	-121.765710	MSCL, split/photo	describe, sample
29GC	35.733733	-121.765903	MSCL, split/photo	describe, sample
30JPC	35.734248	-121.766113	MSCL, split/photo	describe, sample
31JPC	35.766752	-121.856075	porewater, MSCL, split/photo	describe, sample
32JPC	35.756970	-121.869382	porewater, MSCL, CT, split/photo	describe, sample
33JPC	35.767225	-121.855387	porewater, MSCL, split/photo	describe, sample
34JPC	35.608703	-121.843190	porewater, MSCL, split/photo	describe, sample
35JPC	35.560735	-121.713473	porewater, MSCL, split/photo	describe, sample
36JPC	35.563022	-121.713015	porewater, MSCL, split/photo	describe, sample
37JPC	35.542640	-121.561642	porewater, MSCL, split/photo	describe, sample
38JPC	35.733063	-121.766493	MSCL, split/photo	describe, sample
39JPC	35.776725	-121.812822	porewater, MSCL, split/photo	describe, sample
40JPC	35.782235	-121.817752	porewater, MSCL, split/photo	describe, sample

3 Results

In this section we detail the results of surficial (surface-ship and AUV bathymetry) and subsurface (MCS, Chirp, and AUV Chirp) mapping of structure and stratigraphy, and highlight some specific observations of the pockmark field. We also provide preliminary analysis of the piston/gravity core and ROV vibracore data (MSCL, CT scan, photograph, porewater, ^{14}C , and compositional analysis) from the pockmark field and channel areas.

3.1 Subsurface stratigraphy

In this section, we showcase interpolated, gridded data derived from mapping of subsurface *horizons* (mappable seismic reflections that feature identifiable amplitude characteristics or relationships), some of which represent *unconformities* (mappable seismic reflections with amplitude characteristics that suggest breaks in geologic time) in high-resolution MCS data. While MCS data only allow for mapping of seismic reflections (i.e., the acoustic response of the geology), we assume that the seismic reflections indicate geologic layers. Mapping seismic reflections and their characteristics thus helps to identify geologic events (such as erosion, gas accumulation, deformation, etc.) and interpret these events in relative time and space. In the map figures, we show the interpolated gridded seismic reflection horizons (i.e., *surfaces*), categorized by their physiographic region (see Fig. 3; pockmarks, basin, SLB north, SLB south, and regional). The names of the subsurface horizons and corresponding map surfaces use the following naming convention (e.g., Pockmark Unconformity 2): 1) physiographic region, 2) a one- to two-word description (e.g., unconformity), and 3) a number that represents the relative timing of the surface in its respective region, with one (1) being the oldest. Relative timing was determined by interpreting the geologic and stratigraphic relationships between surfaces, with the oldest surfaces located deepest stratigraphically and vice versa. In some cases, a letter appended to the relative age number indicates two surfaces (e.g., 4a and 4b) that are indistinguishable in age due to their mapped extents and the available data. Example MCS crossings through each of the regions accompany the mapped surface figures and show what each of the mapped surfaces look like in the subsurface (though note that the selected MCS profiles do not cross through some surfaces with relatively small geographic spatial extents).

In the pockmark region, we map 10 distinct horizons in the subsurface (Fig. 4, Fig. 5). Figure 6 shows examples of MCS and Chirp profiles crossing the pockmark field. The Pockmark Deep 1 surface marks the base of acoustic reflections and covers the majority of the northern pockmark area. Pockmark Unconformity 2 and Pockmark Surface 3 are unconformable and acoustically high-amplitude (*bright*) reflection surfaces, respectively, that appear within a folded *package* (series of layers) that onlaps onto the acoustic basement. Pockmark Unconformity 4a marks the top of that folded package, and Pockmark Local Surface 4b is a local unconformity within the western part of the study area. Pockmark Unconformity 5a is a relatively extensive surface marking the top of a package that onlaps the folded reflections beneath it, and Pockmark Local Surface 5b, a local surface located just north of SLB, is roughly contemporaneous. Above 5a and 5b, we map localized high-amplitude reflections including Pockmark Bright 6, a reflection surface that exhibits punctuated high-amplitude reflections within an otherwise fairly acoustically transparent package; these are acoustic characteristics typical of gas deposits (e.g., Holbrook et al., 2002). Pockmark Surface 7 is another regionally extensive, relatively high-amplitude reflection surface, and while Pockmark Surface 7 does not have the same punctuated high-amplitude reflections of Pockmark Bright 6, Pockmark Bright 8 is similar to Pockmark Bright 6 in that it shows punctuated areas of high-amplitude reflections throughout the pockmark region.

In the basin region to the east of SLB, we map 6 distinct horizons in the subsurface (Fig. 7). We show an example MCS crossing in Figure 8. This area exhibits three deep surfaces that represent acoustic

basement in different sub-areas of the region – from deepest/oldest to shallowest/youngest, they are Basin Deep 1, Basin Deep 2, and Basin Deep 3. The acoustic basement appears along different surfaces due to heterogeneous lithology, which results in differing acoustic penetration throughout the region. Deformed stratigraphy is visible just beneath Basin Deep 3 in most areas. Basin Unconformity 4 caps an acoustically transparent package that onlaps onto Basin Deep 3. Basin Erosion 5 represents an erosional unconformity of another folded, fairly acoustically transparent package that extends along the eastern edge of SLB. Basin Bright 6 is located near the southern cluster of pockmarks along the eastern flank of SLB and exhibits punctuated high-amplitude reflections similar to those of the other bright surfaces in the pockmark region (Pockmark Bright 6, Pockmark Bright 8).

In the SLB north region, we map 4 distinct horizons in the subsurface (Fig. 9). We show an example MCS crossing in Figure 10. We map two deep surfaces (SLB North Deep 1 and SLB North Deep 2). The SLB North Deep 1 surface is much more local than SLB North Deep 2, and marks the top of part of the acoustic basement. SLB North Deep 2 is an unconformity surface with fairly good regional coverage and marks the top of weakly visible, highly deformed and tilted stratigraphy. Above the deep surfaces, SLB North Unconformity 3 caps stratigraphy that infills and onlaps lows in the basement topography. SLB North Local Surface 4 is the youngest mapped surface in the area and covers a small region in the northernmost area of SLB.

In the SLB south region, we map 7 distinct horizons in the subsurface (Figs. 11 and 12). We show an example MCS crossing in Fig. 13. SLB South Deep 1 marks the top of the acoustic basement in many sub-areas, which is acoustically chaotic and largely homogenous but exhibits weakly reflective, highly deformed strata visible in some sub-areas (Fig. 13). SLB South Unconformity 2a and 2b both mark the top of different areas of folded, deformed stratigraphy atop the basement, and both surfaces have fairly localized, non-overlapping spatial coverage. SLB South Unconformity 3a caps another deformed package with fairly regional coverage along southwestern SLB, and the contemporaneous SLB South Canyon 3b surface marks an unconformity in the canyons and gullies located up and down the western flank of SLB. The SLB South Unconformity 4 surface sits along the top of more folded stratigraphy, above which sits a characteristically acoustically transparent package with a different orientation of folding. SLB Erosion 5 marks the erosional top of that shallow transparent, folded package.

We additionally map 5 horizons that cross into multiple physiographic regions or indicate geologic processes happening in several different physiographic regions (Fig. 14). These seismic reflection surfaces include the seafloor (Regional Seafloor; see also MCS data in Figs. 6, 8, 10 and 13) and a shallow onlap surface (Regional Unconformity), which appears in the pockmark and basin physiographic regions (see also MCS data in Figs. 6 and 8). Surfaces that indicate regional processes include the Regional Bright surface (see MCS data in Fig. 6), which appears in patches of the pockmark and basin physiographic regions; this surface is a discontinuous, locally high-amplitude reflection surface exhibiting high-frequency attenuation (a degree of acoustic blanking) beneath it (Fig. 6). Lower-resolution crustal-scale legacy MCS data from the same location also shows high-frequency attenuation below and a reverse-polarity reflection along the Regional Bright horizon. We also map buried channels (Regional Paleochannel surface) in the study area, which appear in the pockmark and basin physiographic regions (see MCS data in Fig. 8 for an example). Lastly, we map a small area with acoustically chaotic, blocky layers that possibly represent mass-transport deposits (MTDs) in the basin area east of SLB (Fig. 8).

Lastly, we present a minimum sediment thickness map (Fig. 15) that we base on mapping of high-resolution MCS data (see Methods above for further processing details; also note that the study area outside of our mapping is largely devoid of sufficient, consistent-quality, high-resolution data with which to constrain sediment thickness). This map shows the difference between the most regionally extensive deep surfaces (those that include basement picks) and the seafloor in the study area. The thinnest sediment cover (at or approaching ~0 m thickness) is atop SLB, especially along the central area just west

of the eastern edge of the bank. Thickest sediment cover (approaching ~700 m thickness) is in the northernmost pockmark area, and in the northeast closest to the coastline.

3.2 Fault structure and scarps mapping

We present a combination of surficial and subsurface mapping in a combined fault map (Fig. 16; see Methods for further details on interpretation parameters). Age and fault activity interpretations are based on the stratigraphic model of McCulloch et al. (1982), which itself is based on correlations of regional crustal-scale MCS data to an industry exploration well. We map both faults in both Quaternary and pre-Quaternary stratigraphy using bathymetric and subsurface data, and define the fault age based on whether or not the faults offset the seafloor or sediment likely to be Quaternary in age. Some faults exhibit “tectonic” vertical displacements (i.e., basement-involved offsets, untraceable stratigraphy, substantial folding or deformation, and/or abrupt lithology changes across them), although most exhibit small vertical displacements, with seismic reflections offset but still traceable across the fault in the subsurface.

The vast majority of the faults in our study occur within pre-Quaternary stratigraphy with small vertical displacements (Fig. 16; see also MCS data in Figs. 6, 8, 10, and 13). We mapped a few possible Quaternary faults in the pockmark and northern SLB physiographic regions; these faults exhibit mostly small vertical displacements (Fig. 16; see also MCS data in Fig. 10). Some pre-Quaternary faults terminate at or near the seafloor, but do not appear to offset Quaternary sediment, so we classify these structures as pre-Quaternary (Fig. 16; see also MCS data in Figs. 10 and 13). We identify a number of pre-Quaternary faults with tectonic vertical displacements, but only two possible Quaternary tectonic faults, both adjacent to the eastern edge of SLB (Fig. 16). Mapped Quaternary faults are all less than 6 km in length (Fig. 16), whereas pre-Quaternary fault segments approach 26 km in mapped length. The longest, most continuous fault system we map is along the eastern flank of SLB, which features a NW-trending, ~160-m-high scarp with a relatively gentle ~2–10° slope along its ~90-km length. This eastern edge of SLB has been referred to as the Santa Lucia Bank fault (SLBF; e.g., McCulloch, 1987). We map several fault structures along the edge of SLB as continuous, tectonic, pre-Quaternary faults (Fig. 16). An oblique seismic reflection crossing of the eastern edge of SLB (Fig. 17) shows a representative example of the structure and stratigraphy crossing SLBF, as well as the fault scarp itself at the bank edge. The character and structure within the SLBF scarp changes along strike; in some areas the scarp itself is an uplifted bedrock outcrop (as in Fig. 17), and in other areas it is a fold scarp. In all cases along the SLB, the scarp edge is onlapped from the east by flat-lying basin sediment.

Apart from the SLBF, the top of the SLB itself features prominent fault deformation, some of which is exposed at the seafloor (Fig. 16). These faults are again primarily pre-Quaternary and discontinuous, but several bank-top structures exceed 6 km in mapped length and exhibit tectonic vertical displacements in the subsurface (Fig. 16). The AUV bathymetry Chirp data provide further insight into some of the more prominent fault scarps atop SLB (Fig. 18). Like the SLBF, a number of these features appear to be fold scarps and/or basement highs, and scarps and basement highs exhibit vertical relief and lateral offsets at the seafloor (Fig. 18). Bank-top scarps are often onlapped by a thin layer of younger, undeformed, sediment drape (Fig. 18). We note that an apparent lack of mapped faults just west of the SLBF is due to limited high-resolution subsurface data in that area rather than a real lack of fault structures; similarly, between the coast and the SLBF, a large gap in high-resolution data exists (see Fig. 2 for subsurface data coverage).

Lastly, we note that slope-failure scarps, apparent in the available bathymetric data, are common throughout the SLB region and are apparent in the available bathymetric data (Fig. 19). These are distinct from fault scarps because they are generally curvilinear (rather than linear) and often located adjacent to other sediment conduits (like canyon and gully systems). Scarps associated with slope failure and mass-

transport processes are concentrated around the edges of the canyons and gullies along the western edge of SLB and scattered around the other edges of the bank near the relatively steeper (up to $\sim 10^\circ$) slopes in those areas (Fig. 19). We map a small area with a possible MTD complex in the subsurface along northwestern edge of SLB (Figs. 8, 14, and 19), which is adjacent to several mapped edges of mapped surficial scarps. We do not detect any debris fields in the bathymetric data associated with mass-transport processes or associated with scarps.

3.3 Pockmark mapping

We observe pockmark features in both the bathymetric data (Fig. 20) and in varying resolutions of subsurface geophysical data (Fig. 6, Fig. 21). We map just under 5000 distinct pockmarks across two physiographic regions, the pockmark region and just east of SLB and south of the San Simeon channel in the basin region, covering a total area of nearly 1300 km² (Fig. 20). This makes the Big Sur pockmark field the largest known pockmark field in North America (e.g., Mazzini et al., 2017). The pockmarks average ~ 5 m deep and ~ 175 m in diameter (Lundsten et al., 2019), and are located at water depths ranging from ~ 500 to 1400 m. In addition to mapping the pockmark locations, we also calculate relative spatial density of the pockmarks within the pockmark fields (Fig. 20).

In the subsurface, MCS data show that pockmark features exhibit “trails” of localized high-amplitude reflections beneath the seafloor depressions that extend up to ~ 100 m into the subsurface (Fig. 6). A number of these trails appear to root out into Pockmark Surface 7 in the eastern part of the pockmark field, and the stratigraphically deeper Pockmark Unconformity 5a in the western part of the pockmark field (Fig. 6). We also map some features in the subsurface that appear to be pockmarks buried beneath 10s of meters of sediment (Fig. 6). These “old pockmarks” appear clustered on the northeastern edge of the surficial pockmark field (Fig. 20). In the pockmark physiographic region, the subsurface data also show several horizons punctuated by high-amplitude reflections within the upper ~ 100 m of sediment (Pockmark Bright 6 and 8, Figs. 5 and 6; Basin Bright 6, Figs. 7 and 8; Regional Bright, Figs. 6 and 14).

AUV bathymetry and Chirp data reveal detailed information about the morphology of the pockmarks and the shallow subsurface beneath the modern pockmarks (Fig. 21). The AUV Chirp data show that an acoustically transparent ~ 5 -m-thick drape layer tops the modern pockmarks at the seafloor, and localized higher amplitude reflections appear periodically throughout the subsurface beneath the surficial pockmark depression (Fig. 21). There are several subsurface horizons that correlate between these high-amplitude reflection “events” in adjacent pockmarks (Fig. 21). Another interesting feature is that pockmark features appear to have undergone discrete shifts in location at these “event” horizons and often (though not always) in a net southeasterly direction (Fig. 21). Using MCS data, we have measured a net lateral shift over time of up to 300 m for some pockmarks.

3.4 Preliminary results from core analysis

Vibracores and piston cores were collected throughout the study area, targeting the Lucia Chica and San Simeon channel systems, pockmarks, fault systems atop and along SLB, and paleoceanographic sites (designed specifically for paleoceanographic studies and not discussed further in the present study) within the sedimentary basins. At the time of writing this report, core analyses are in progress and have not yet been completed (Table 1); however, we present preliminary analysis and examples of priority cores where some stages of processing have been completed, focusing on the piston core dataset.

Early analysis of piston and gravity core data collected aboard the R/V *Bold Horizon* in 2019 show some interesting sedimentary characteristics. We highlight photograph and CT scan data from the example piston core 23JPC taken inside a pockmark (Figs. 22, 23). This core shows several sand layers with sharp

basal contacts and fining-upward grading (Figs. 22, 23), characteristic of turbidite sequences (Bouma, 1962). In analyses of porewater geochemistry, we specifically targeted sulfate and chloride concentrations. Profiles of sulfate concentrations versus sub-bottom depths are a proxy that is sensitive to the upward methane flux (e.g., Borowski et al., 1999). Porewater analyses from pockmark cores 23JPC and 32JPC show a relatively abrupt decrease in sulfate in both cores at 4–5 m depth, distinct from the other pockmark cores, which otherwise show slow rates of sulfate depletion with depth and consistent sulfate gradients down core (Fig. 24). In both 23JPC and 32JPC, the relatively abrupt change in sulfate gradient occurs at the level of lithologic changes indicated by the magnetic susceptibility and density logs. The split 23JPC core reveals sand layers at the depths corresponding to the relatively abrupt sulfate decrease (Figs. 22, 23). We observe similar inflections in sulfate gradients at ~4 m depths in some of the cores from the Lucia Chica channel, which also correspond with shifts in the density logs (Fig. 25). Chloride values in all cores from porewater analysis were similar to the overlying seawater and did not change with depth. Lastly, we note that although gas squeezes were performed on whole-round sections near the base of the pockmark cores, no gas was recovered from any of these samples nor was methane detected in the porewater.

Elsewhere, MSCL and porewater analysis from cores in the Lucia Chica and San Simeon channel systems also show evidence for repeated high-density layers down section (Lucia Chica channel example data shown in Fig. 25). Other piston cores ostensibly collected for paleoceanography studies downslope of SLB also reveal some highly variable magnetic susceptibility and density logs (Fig. 26), potentially indicating sandy layers. A transect of 2019 MBARI R/V *Western Flyer* vibracores collected along one of the fault scarps atop SLB (example core photograph data in Fig. 27; core locations shown in Fig. 18) show considerable layering; more analysis is required to correlate across these cores and better understand the composition, stratigraphy, and age of these sediments. Lastly, we note that preliminary analysis of seabed sand and rock samples reveals evidence for glauconite in the SLB bank top area, which can be diagnostic of longevity of exposure to seawater.

4 Discussion

4.1 Fault hazards

We interpret the majority of faulting and deformation structures in the study area as likely to be pre-Quaternary (Fig. 16), and thus of low risk to seabed stability. Key supporting observations include little to no deformation occurring within Quaternary sediment (McCulloch et al., 1982) and undeformed sediment drape conforming to underlying topography in the SLB area (e.g., Fig. 18). Subsurface mapping reveals deformation throughout the study area, including folding and faulting, but primarily in the SLB (e.g., Figs. 10, 13, and 17). The SLB seems to be an uplifted, tilted, deformed, and lithified sedimentary bedrock structure topped in some areas by deformed sedimentary packages (e.g., Fig. 17), and cut by numerous discontinuous and blind faults (e.g., Fig. 16). The acoustic basement in our dataset is generally shallow and sediment cover is thin across large swaths of SLB (Fig. 15), especially approaching the eastern edge of the bank, which corresponds with the SLBF system (e.g., Fig. 17). Shallow bank-top sediments are Pliocene or older (McCulloch et al., 1982), and preliminary evidence for glauconite in seafloor core and rock samples from the top of SLB implies long exposure of the seafloor to seawater. These observations imply that little Quaternary sedimentation has taken place on the SLB, perhaps due to its elevation above the basin to the east (~160 m) and lack of nearby terrestrial sediment (i.e., channels).

Together, our observations suggest that 1) formation of the SLB in a previous, pre-Quaternary tectonic regime and 2) little to no Quaternary tectonic deformation of the bank itself. These interpretations are consistent with previous studies suggesting that the SLB was formed as part of an early Tertiary

subduction complex, which generated lithified sedimentary rocks composition analogous to the Franciscan Complex (McCulloch et al., 1980, 1982; McCulloch, 1987; Namson and Davis, 1990). Stratigraphy above the SLB bedrock exhibits different amounts and types of deformation (e.g., Figs. 10, 13, and 17) as well as different orientations of faulting (Fig. 16), supporting a concept of multiple phases of pre-Quaternary deformation. Later stages of shallower deformation on the bank may have formed during the Miocene extension and basin formation, post-Miocene (5–3 Ma) convergence, and/or modern transpression (e.g., McCulloch, 1987). We suggest that SLB was uplifted by the early Pleistocene, and its elevation or shallow currents subsequently prevented sedimentary and pelagic deposition; thus, Quaternary sediment history is largely missing in areas exhibiting intense faulting.

Because it is likely a pre-Quaternary structure, the SLBF is unlikely to pose substantial seismic hazard. The SLBF has long been considered a potentially active fault, perhaps accommodating some component of strike-slip motion across the larger San Andreas fault right-lateral transform system (McCulloch, 1987; Dickinson et al., 2005; Johnson et al., 2018). The SLB scarp itself is largely uplifted bedrock (e.g., Fig. 17) and presents as a fold scarp in other areas. The SLB likely contains the oldest geologic units in our study area (McCulloch et al., 1982), and younger, flat-lying stratigraphy in the basins to the north and east of SLB consistently onlap the eastern uplifted, scarp-like edge of SLB (e.g., Fig. 17). Little to no recorded seismicity exists in the SLB region, especially the northern part (Fig. 1); the closest two historical events (M5.8 and M6.0 thrust events in 1969; Fig. 1) have been located just southwest of the SLB (Gawthrop, 1975). So, despite the ~160-m scarp suggesting substantial tectonic offsets across the SLBF, our results together suggest that the SLBF is not currently accommodating tectonic offsets.

We map several potential Quaternary faults in our study that vertically displace shallow, flat-lying stratigraphy (Fig. 16), although poor age control on the shallow stratigraphy prevents confident interpretation that these faults offset Quaternary deposits. If these faults are in fact Quaternary, subsurface data show that the majority are small-displacement, and the two that exhibit tectonic displacements (along the SLBF system; see Fig. 16) are short in mapped length (<3 km long) and discontinuous. If not Quaternary, at a minimum, these faults seem to represent a later phase of SLB deformation, as they are more vertical (suggesting strike-slip) and exhibit less cumulative deformation (e.g., folding) than the pre-Quaternary faults. We also note that Quaternary reactivation of pre-Quaternary, pre-existing fault structures is possible, though difficult to quantify given the difficulty of seismic imaging in the SLB physiographic regions and the lack of recent seismicity (Fig. 1). Continuing analysis of core data (e.g., age dating) will better constrain the age model for the shallow stratigraphy and recent fault activity.

While it appears unlikely that there are substantial Quaternary structures in the SLB area, evidence for sands downslope of SLB in core data (Fig. 26) implies that shaking along nearby Quaternary fault systems, like the San Andreas or San Gregorio-Hosgri faults (Fig. 16), may trigger mass sediment transport along the edges of the SLB. Turbidity flows would otherwise be unexpected so far from sediment distribution systems like channels, and the SLB is too deep (just over 400 m at its shallowest) to have been subaerial during recent sea-level lowstands. Thus, any sands in cores are thus very likely to have been transported via mass wasting processes. More analysis of the cores is required to date the deposits, determine provenance and confirm the sands derive from SLB, and to examine evidence for known historical earthquakes, specifically the 1927 Lompoc, California, M7.0 earthquake, for which the source fault is uncertain (Gawthrop, 1978; Helmerberger et al., 1992; Satake and Somerville, 1992). Specifically, ^{14}C and compositional/grain size analyses of core samples will be useful for determining first-order sourcing of transported sands (please refer to Table 1 for piston and gravity core processing status as of 18 June 2021).

4.2 Pockmark hazards

Our results suggest that the pockmark physiographic region does not appear to be associated with high methane fluxes, and that pockmarks are not currently sites of active seepage. As a group, all the measured porewater sulfate profiles within the study region, both within the pockmark fields and outside them, show low to modest rates of sulfate depletion with depth. Two of the five piston cores taken in the center of pockmark depressions (23JPC and 32JPC) show an inflection in sulfate gradients at 4–5 m depths (Fig. 24); the other three are indistinguishable from nearby cores taken in between pockmarks. Additionally, analysis of surface-ship water-column data (from the 2018 *Rainier* survey) reveals no evidence of seeps in the water column. In a different coring study, Paull et al. (2002) also found no evidence of methane or exotic fluids in the upper ~50 ka record of pockmark sediments, concluding that the pockmarks were geochemically identical to the surrounding seafloor. Thus far our study provides no evidence to contradict Paull et al. (2002).

While we have no new evidence to suggest the pockmarks present a current threat to seafloor stability, there is substantial uncertainty surrounding the processes leading to pockmark formation and how recently these processes were active. Our geophysical analysis suggests that it is possible the pockmarks exist due to gas migration processes, perhaps forming and re-forming in infrequent, periodic events over time. MCS data suggest that the pockmarks have persisted in the area for about the last ~1 Myr based on a sedimentation rate of ~10 cm per 1000 yr (Paull et al., 2002) in the pockmark field, assuming that pockmarks extend into the subsurface up to 100 m (as suggested by our MCS data; Fig. 6). Our high-resolution geophysical data, as well as crustal-scale legacy MCS data from the same area, show acoustic bright spots along some subsurface horizons in the shallow subsurface in the pockmark area, reverse-polarity reflections, and high-frequency attenuation beneath some bright layers (e.g., Fig. 6). These characteristics are consistent with the occurrence of interstitial gas accumulation in the shallow subsurface (e.g., Holbrook et al., 2002). Some high-amplitude “event” layers seem to correlate between different pockmarks in the subsurface as well as discrete shifts in pockmark locations (e.g., Fig. 21), suggesting that regional processes lead to pockmark formation and infill periodically over time. We speculate that one possible source of the subsurface “events” may be changing relative sea level, which could modulate the release of subsurface methane via changes in hydrostatic pressure. Further analyses, specifically sampling, age dating, stable isotope, and compositional analyses, are needed to confirm the sediment age model and the geochemistry of the deeper (4–7 m) pockmark sediments, which may have diagenetic evidence suggesting elevated methane concentrations in earlier times.

Pockmarks are relatively common features worldwide, and generally attributed to some form of fluid and/or gas discharge, but are poorly understood. Theoretically, pockmarks can form via any mechanism that removes sediment from or prevents it from being deposited in a localized area (e.g., Paull et al., 2002). We remain open to alternative possibilities for pockmark formation such as subsidence along subsurface faulting, biologic disturbances to the seafloor, and non-methane diagenetic processes (e.g., opal-A to opal-CT). It is also possible that sandy sedimentary layers from turbidity flows or mass wasting lead to the acoustic bright spots we observe in seismic reflection data (Figs. 6 and 21). Sand layers may also lead to the relatively abrupt sulfate reduction (Fig. 24) and spikes in density and magnetic susceptibility (Fig. 24) we observe in the pockmarks; these characteristics are similar to observations in the Lucia Chica channel, where we would expect sand (Fig. 25). In comparing pockmark maps to regional structures, we do not observe a notable correlation between faulting and pockmark occurrence (see Figs. 16 and 20), although a relative lack of faulting in the pockmark areas could be related to the relative difficulty of mapping faults within the disturbed amplitudes beneath the pockmark fields. Intriguingly, there does seem to be a qualitative correlation between thicker sediment (basement lows) and denser pockmarks (see Figs. 15 and 20), although the reason is not clear. Further analysis of the pockmarks and

subsurface mapping is needed to better understand the potential relationships between faulting, sediment thickness, and pockmarks.

4.3 Sediment gravity flows hazards

Among the largest threats to seabed stability in our study area are mass wasting and sediment gravity flow processes, some of which (channel activity, earthquake-induced sediment transport) we have identified as Quaternary processes. Our study includes several examples of evidence for sediment gravity flows, including the sand deposited downslope of SLB described above (see Fig. 26), sandy layers in pockmark cores (see Figs. 22, 23, and 24), and in the Lucia Chica and San Simeon channel systems (see Fig. 25). We assume that sand deposits downslope of SLB were potentially triggered by shaking from nearby earthquakes and transported by gravity downslope. Preliminary radiocarbon dating of cores from the side of the San Simeon channel, where multiple seismic reflections truncate at the seafloor, suggests that sediment flows deposited sediment on the levee as recently as ~18.8 ka (Dobbs et al., 2020) during the Pleistocene sea-level lowstand. Outside of the channels, we also map evidence for mass-transport features, including scarps clustered near canyon and gully heads and at the edges of SLB and evidence for MTDs in the subsurface near the northeastern flank of SLB (Fig. 19), although the ages of these features is not known. These results suggest that mass wasting processes play a role in sediment transport in the study area, though perhaps infrequently during the Holocene. Further work, specifically ^{14}C dating of existing core data, is needed to better understand the timing of deposition of the sandy layers found in numerous cores throughout the study area (e.g., Figs. 22, 23, 24, 25, and 26).

5 Conclusions

This report provides baseline geologic interpretation of the south-central California outer continental shelf (OCS) using comprehensive high-resolution sub-bottom, seafloor, and sampling data for the first time. Our results from surficial and subsurface geophysical analysis in the California Deepwater Investigations and Groundtruthing (Cal DIG) I study area include interpretations of structure and stratigraphy, faults and pockmark features, and preliminary results from the groundtruthing core studies. We interpret minimal current geohazards in the study area from local fault or pockmark activity but note that numerous fault structures throughout the region have potential to become reactivated; more work is needed to better understand the origins and recent activity of the Big Sur pockmark field. Mass wasting along the edges of Santa Lucia Bank (SLB) during earthquakes, as well as sediment transport down the Lucia Chica and San Simeon channels, present potential (although still likely infrequent) hazards to seabed stability in the study area. These results will inform marine planning, the viability of offshore development, and improve our understanding of shallow geologic hazards and sedimentary processes. In summary:

1. We find limited evidence for Quaternary fault activity, though we do find intriguing evidence for turbidites along the edge of SLB, perhaps triggered by earthquakes along near-shore transcurrent faults like the San Gregorio-Hosgri fault zone. Most deformation we observe is likely pre-Quaternary, and the SLB is likely a remnant of Tertiary subduction complex.
2. Our results thus far indicate little to no evidence for recent fluid or gas advection in the Big Sur pockmark field, but more analysis of existing core data (i.e., compositional and stable isotope analysis) is needed to understand these enigmatic features and the nature of potential gas accumulations we mapped in the subsurface beneath the pockmark fields.
3. We summarize evidence for mass wasting and sediment transport processes, including seafloor scarps and sand-rich turbidites in cores throughout the study area. While more work (i.e., compositional and dating analysis) is needed to understand the timing and sources of the numerous sand deposits,

preliminary results suggest that sediment flows through channels were last active in the late Pleistocene, and that mass sediment transport has been infrequent in the Holocene.

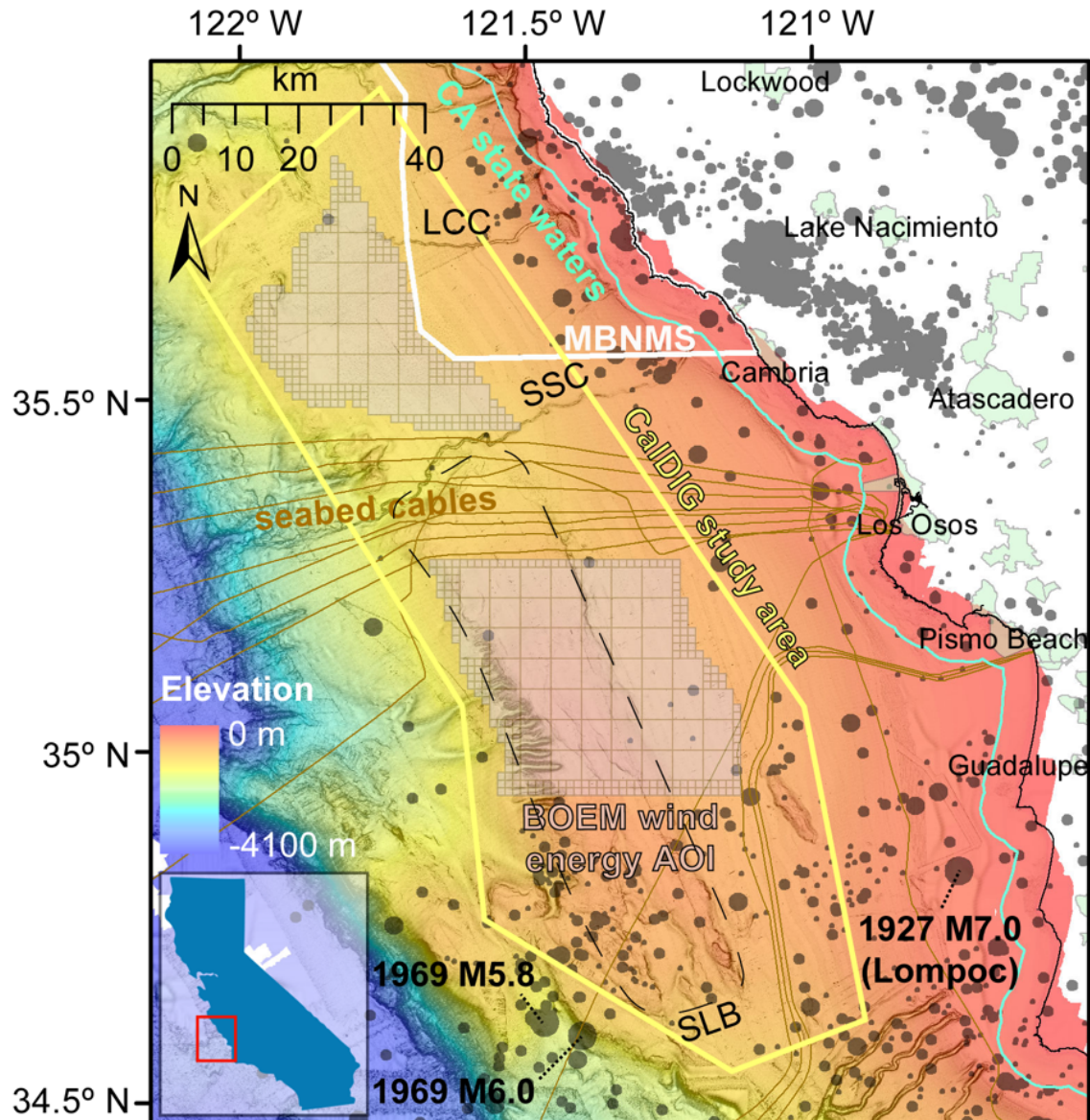


Figure 1. Region of study offshore of Morro Bay, central California.

Figure shows the location of the California Deepwater Investigations and Groundtruthing (Cal DIG) I study area offshore of south-central California (yellow outline). Seismicity since 1900 has been plotted as semi-transparent gray circles that scale in size with magnitude from M2.5 to M7.0; the M5.8 and M6.0 events in 1969 and the M7.0 Lompoc earthquake of 1927 are called out specifically on the figure. Also on the map are the approximate area of the Santa Lucia Bank (SLB; black dashed outline), the extents of Monterey Bay National Marine Sanctuary (MBNMS; white line), the extents of California State waters (blue-green line), the locations of seabed cables (brown lines), the modern coastline (black line), and onshore landmarks (pale green shapes with black text labels). Two semi-transparent pink polygons mark areas for potential future wind energy leasing by BOEM (BOEM, 2018; <https://boem.gov/california>). The inset in the lower right shows the location of the map relative to the State of California. The bathymetry basemap is a semi-transparent merged grid of surface-ship bathymetry provided by Monterey Bay Aquarium Research Institute (MBARI) overlain on a grayscale slope map. AOI – areas of interest. LCC – Lucia Chica channel. SSC – San Simeon channel.

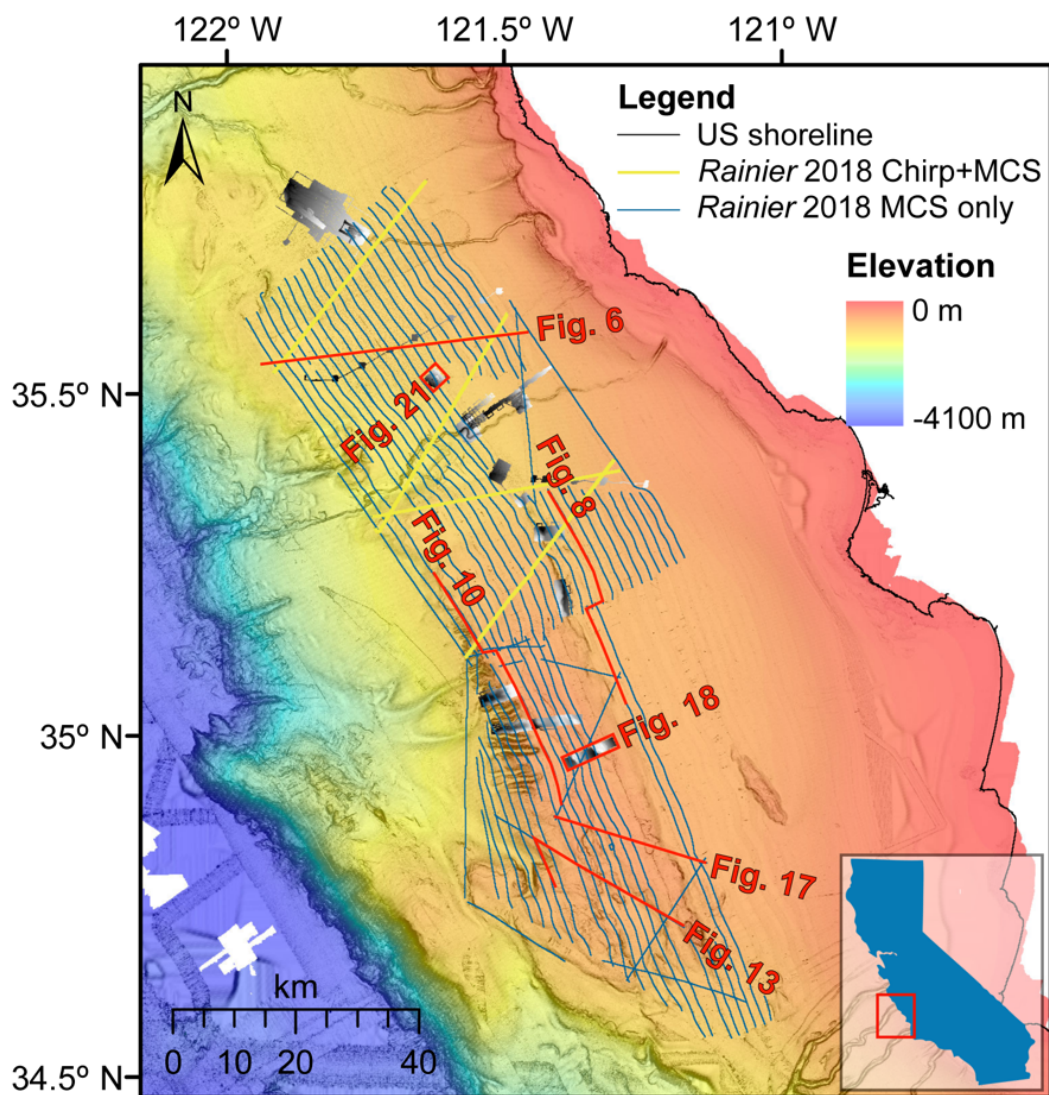


Figure 2. Map of geophysical data.

Figure shows the locations of subsurface geophysical data collected by the National Oceanic and Atmospheric Administration (NOAA) Ship *Rainier* in August–September 2018 (see map legend for details) and surficial and subsurface geophysical data collected by the autonomous underwater vehicle (AUV) aboard the Monterey Bay Aquarium Research Institute (MBARI) R/V *Rachel Carson* in 2018–2019 (small grayscale grid patches). Note that these grayscale bathymetry grids also include coincident MBARI Chirp sub-bottom profile data. The inset in the lower right shows the location of the map relative to the State of California. The bathymetry basemap is a semi-transparent merged grid of surface-ship bathymetry provided by MBARI overlain on a grayscale slope map and includes bathymetry data also collected by the NOAA Ship *Rainier* during the August–September 2018 geophysical survey. Figure extents are the same as those in Figs. 1 and 3. Locations of Figs. 6, 8, 10, 13, 17, 18, and 21 outlined in red.

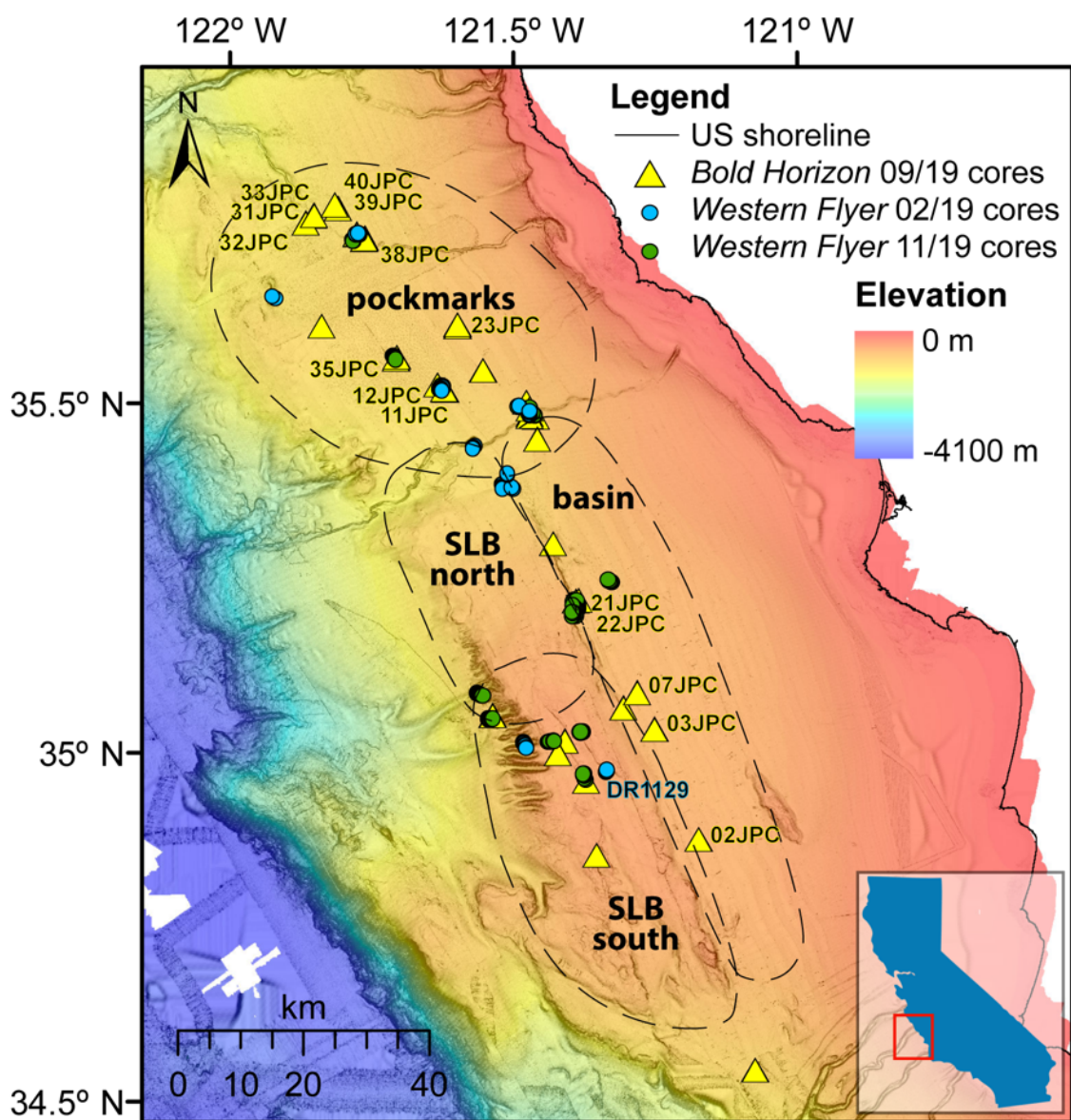


Figure 3. Map of sampling data.

Figure shows the locations of piston and gravity cores collected by the R/V *Bold Horizon* in September 2019 and vibracores and samples collected by the Monterey Bay Aquarium Research Institute (MBARI) remotely operated vehicle (ROV) Doc Ricketts aboard the R/V *Western Flyer* in February 2019 and November 2019 (see map legend for details). Approximate extents of physiographic regions discussed throughout the report have been labeled and outlined with black dashed lines. The inset in the lower right shows the location of the map relative to the State of California. The bathymetry basemap is a semi-transparent merged grid of surface-ship bathymetry provided by MBARI overlain on a grayscale slope map. Figure extents are the same as those in Figs. 1 and 2. Cores highlighted in the report have been labeled (e.g., 02JPC).

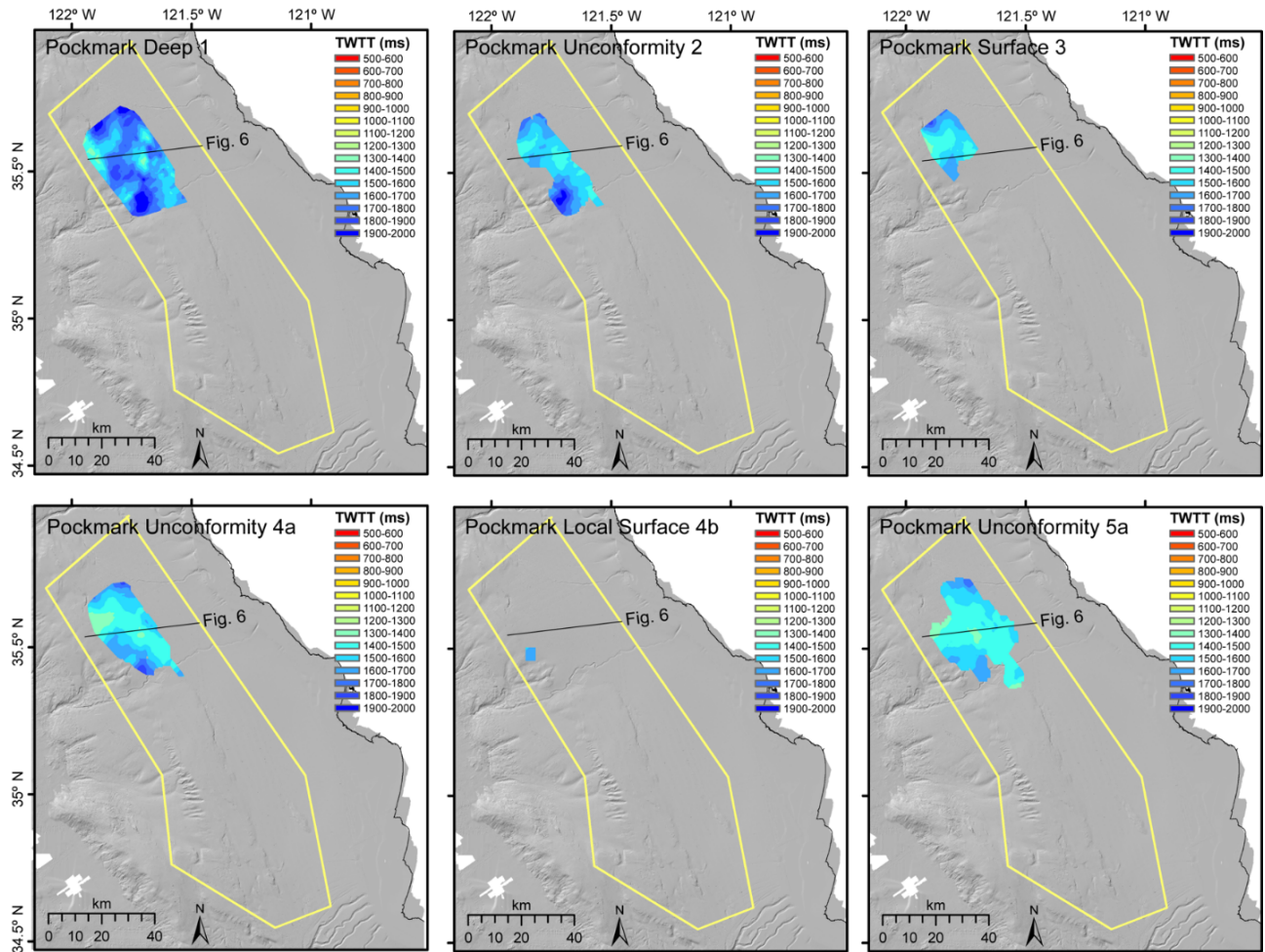


Figure 4. Maps of gridded subsurface horizons in the pockmark area (1 of 2).

Each labeled panel shows a gridded subsurface horizon located within the pockmark physiographic region of the study area. All surfaces display the same color scale (in two-way travel time, TWTT) to emphasize the relative differences in depth. A labeled black line shows the location of the corresponding seismic crossing in Fig. 6, which has examples of each of the surfaces in the multi-channel seismic (MCS) data, with the exception of Pockmark Local Surface 4b. The California Deepwater Investigations and Groundtruthing (Cal DIG) I study area is shown as a yellow outline, and the basemap is a grayscale bathymetric hillshade image from the merged Monterey Bay Aquarium Research Institute (MBARI) bathymetry map shown in Figs. 1, 2, and 3. The spatial extents of each map matches those of Figs. 1, 2, and 3 to show the regional coverage of each grid.

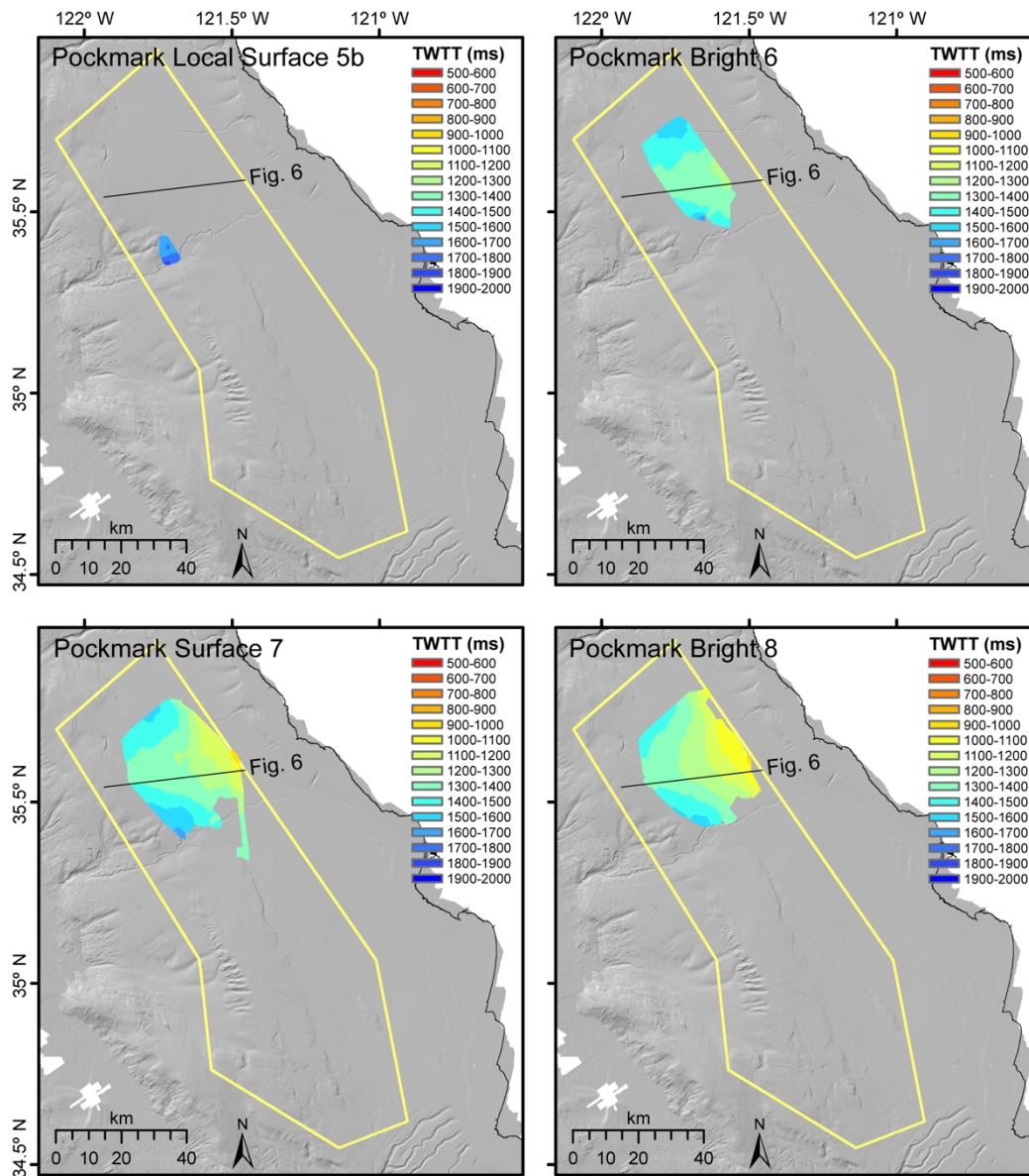


Figure 5. Maps of gridded subsurface horizons in the pockmark area (2 of 2).

Each labeled panel shows a gridded subsurface horizon located within the pockmark physiographic region of the study area. All surfaces display the same color scale (in two-way travel time, TWTT) to emphasize the relative differences in depth. A labeled black line shows the location of the corresponding seismic crossing in Fig. 6, which has examples of each of the surfaces in the multi-channel seismic (MCS) data with the exception of Pockmark Local Surface 5b. The California Deepwater Investigations and Groundtruthing (Cal DIG) I study area is shown as a yellow outline, and the basemap is a grayscale bathymetric hillshade image from the merged Monterey Bay Aquarium Research Institute (MBARI) bathymetry map shown in Figs. 1, 2, and 3. The spatial extents of each map matches those of Figs. 1, 2, and 3 in order to show the regional coverage of each grid.

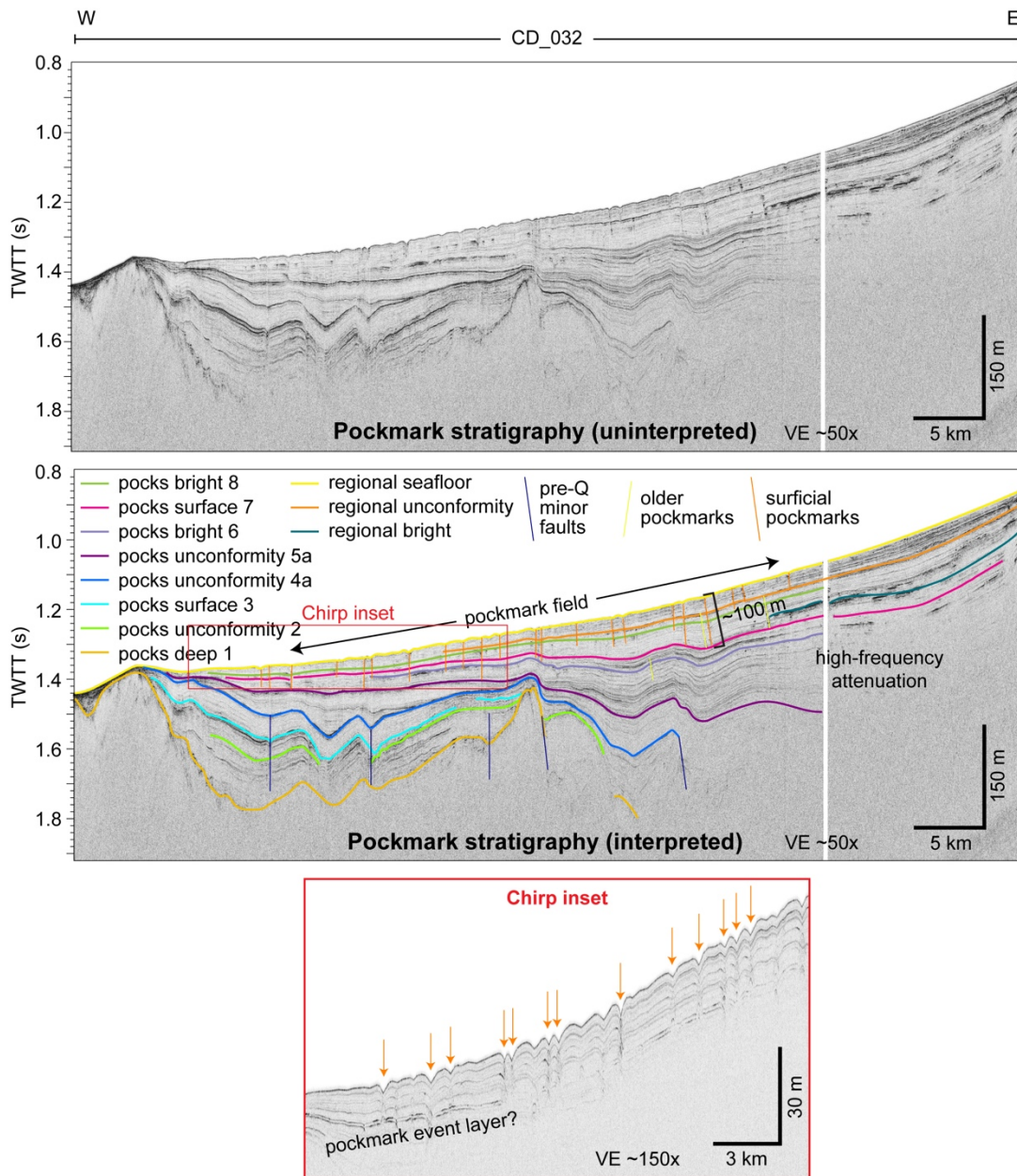


Figure 6. MCS and Chirp images showing subsurface mapping in the pockmark area.

This MCS image (top, center panels) contains seismic reflection data and interpretations along profile CD_032 from the 2018 *Rainier* survey and shows examples of subsurface mapping of horizons located in the pockmark area (line location in Figs. 2, 4, and 5). These horizons were mapped on multi-channel seismic (MCS) data throughout the study area and gridded (grids shown in Figs. 4 and 5). The MCS data are displayed as envelope traces in two-way travel time (TWTT) with an automatic gain control (AGC) window of 0.5 seconds. Coincident 2018 *Rainier* Chirp data are shown in the bottom panel (location outlined in the center MCS panel).

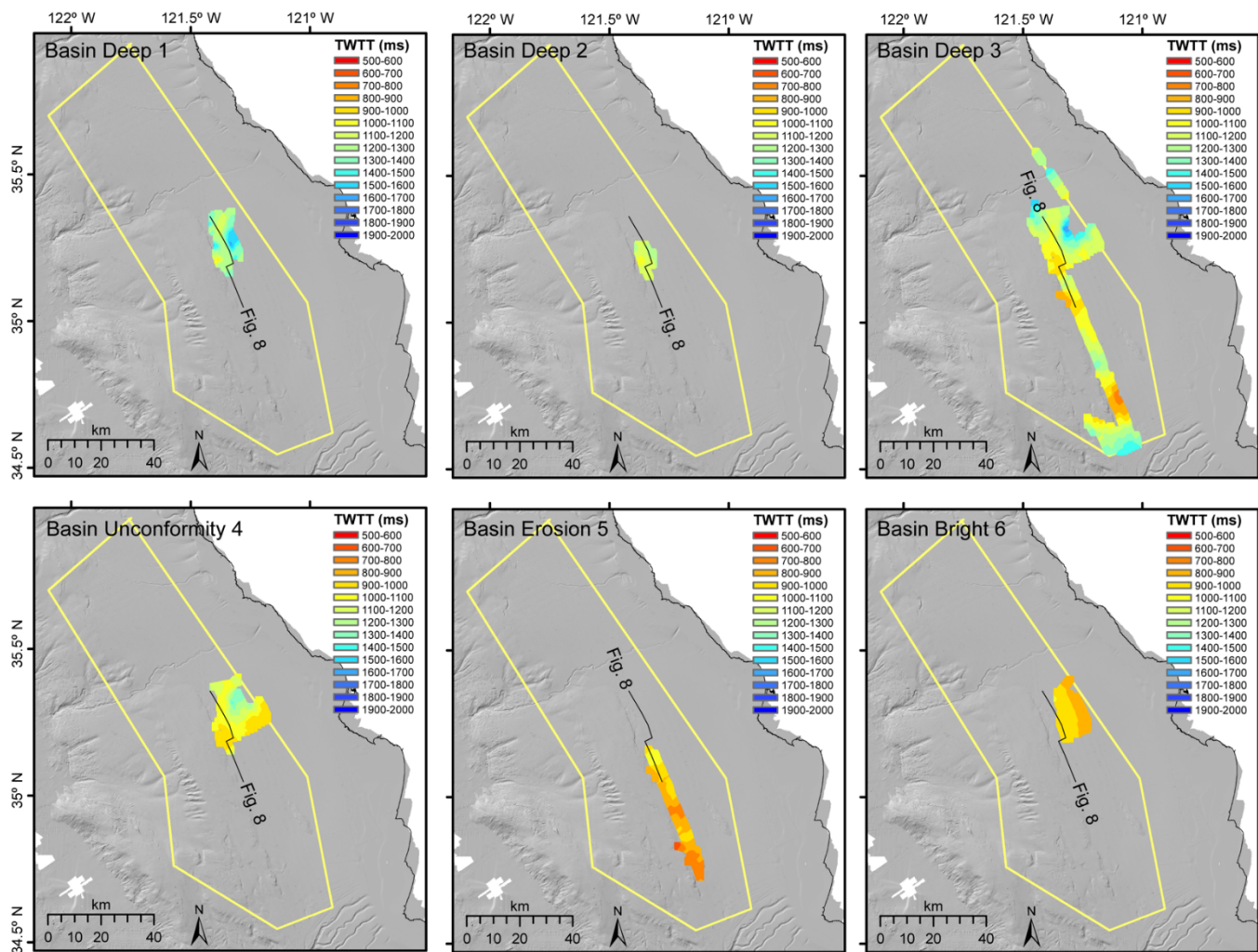


Figure 7. Maps of gridded subsurface horizons in the basin area.

Each labeled panel shows a gridded subsurface horizon located within the basin physiographic region of the study area. All surfaces display the same color scale (in two-way travel time, TWTT) to emphasize the relative differences in depth. A labeled black line shows the location of the corresponding seismic crossing in Fig. 8, which has examples of each of the surfaces in the **multi-channel seismic (MCS)** data. The **California Deepwater Investigations and Groundtruthing (Cal DIG) I** study area is shown as a yellow outline, and the basemap is a grayscale bathymetric hillshade image from the merged **Monterey Bay Aquarium Research Institute (MBARI)** bathymetry map shown in Figs. 1, 2, and 3. The spatial extents of each map matches those of Figs. 1, 2, and 3 in order to show the regional coverage of each grid.

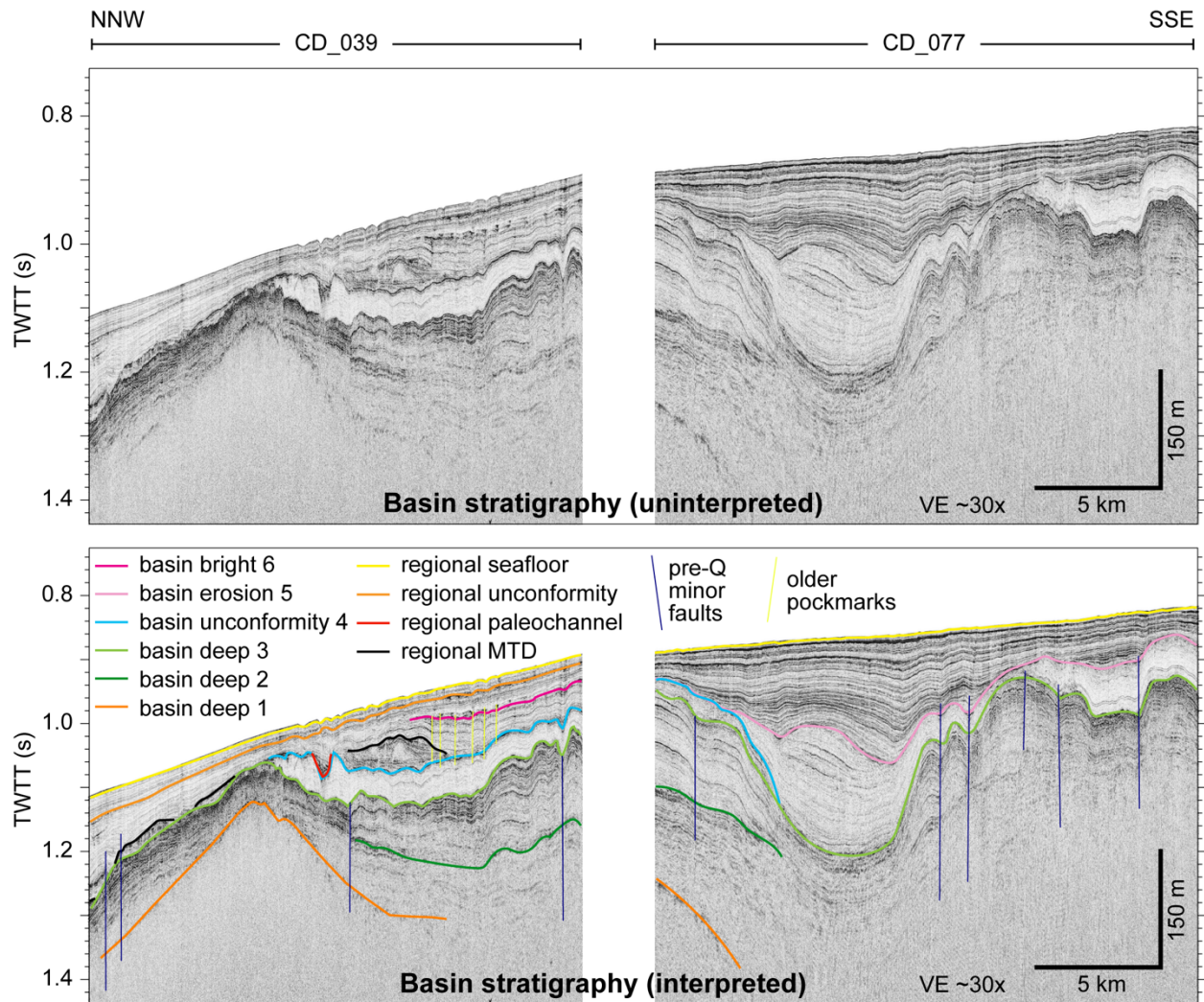


Figure 8. MCS image showing subsurface mapping in the basin area.

This multi-channel seismic (MCS) image contains seismic reflection data and interpretations along sections of 2 profiles (labeled at the top of the image as CD_039 and CD_077) from the 2018 *Rainier* survey and shows examples of subsurface mapping of horizons located in the basin area (line location in Figs. 2 and 7). These horizons were mapped on MCS data throughout the study area and gridded (grids shown in Fig. 7). The MCS data are displayed as envelope traces in two-way travel time (TWTT) with an automatic gain control (AGC) window of 0.5 seconds. MTD – mass-transport deposits.

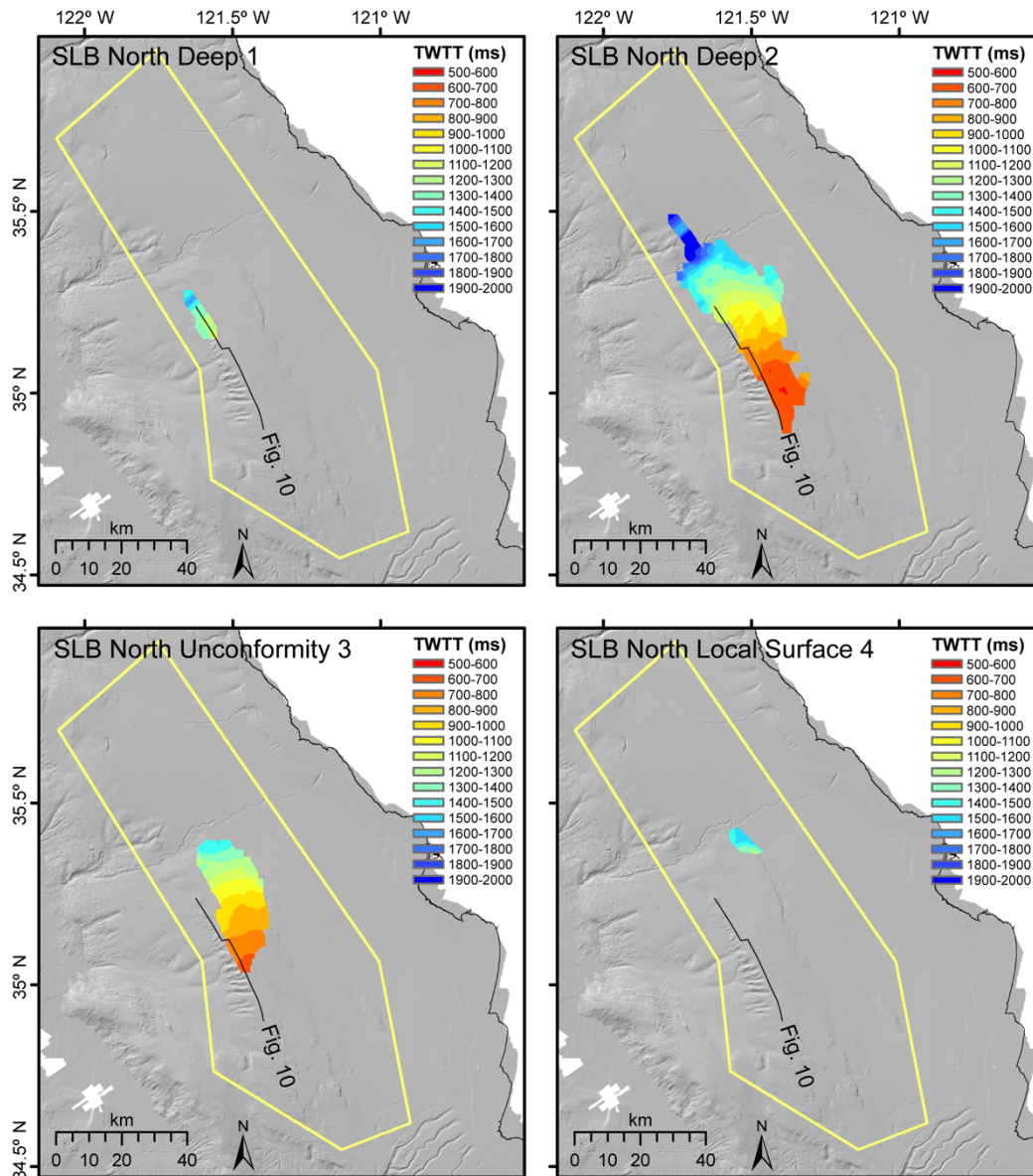


Figure 9. Maps of gridded subsurface horizons in the SLB north area.

Each labeled panel shows a gridded subsurface horizon located within the Santa Lucia Bank (SLB) north physiographic region of the study area. All surfaces display the same color scale (in two-way travel time, TWTT) to emphasize the relative differences in depth. A labeled black line shows the location of the corresponding seismic crossing in Fig. 10, which has examples of each of the surfaces in the multi-channel seismic (MCS) data (with the exception of SLB North Local Surface 4). The California Deepwater Investigations and Groundtruthing (Cal DIG) I study area is shown as a yellow outline, and the basemap is a grayscale bathymetric hillshade image from the merged Monterey Bay Aquarium Research Institute (MBARI) bathymetry map shown in Figs. 1, 2, and 3. The spatial extents of each map matches those of Figs. 1, 2, and 3 in order to show the regional coverage of each grid.

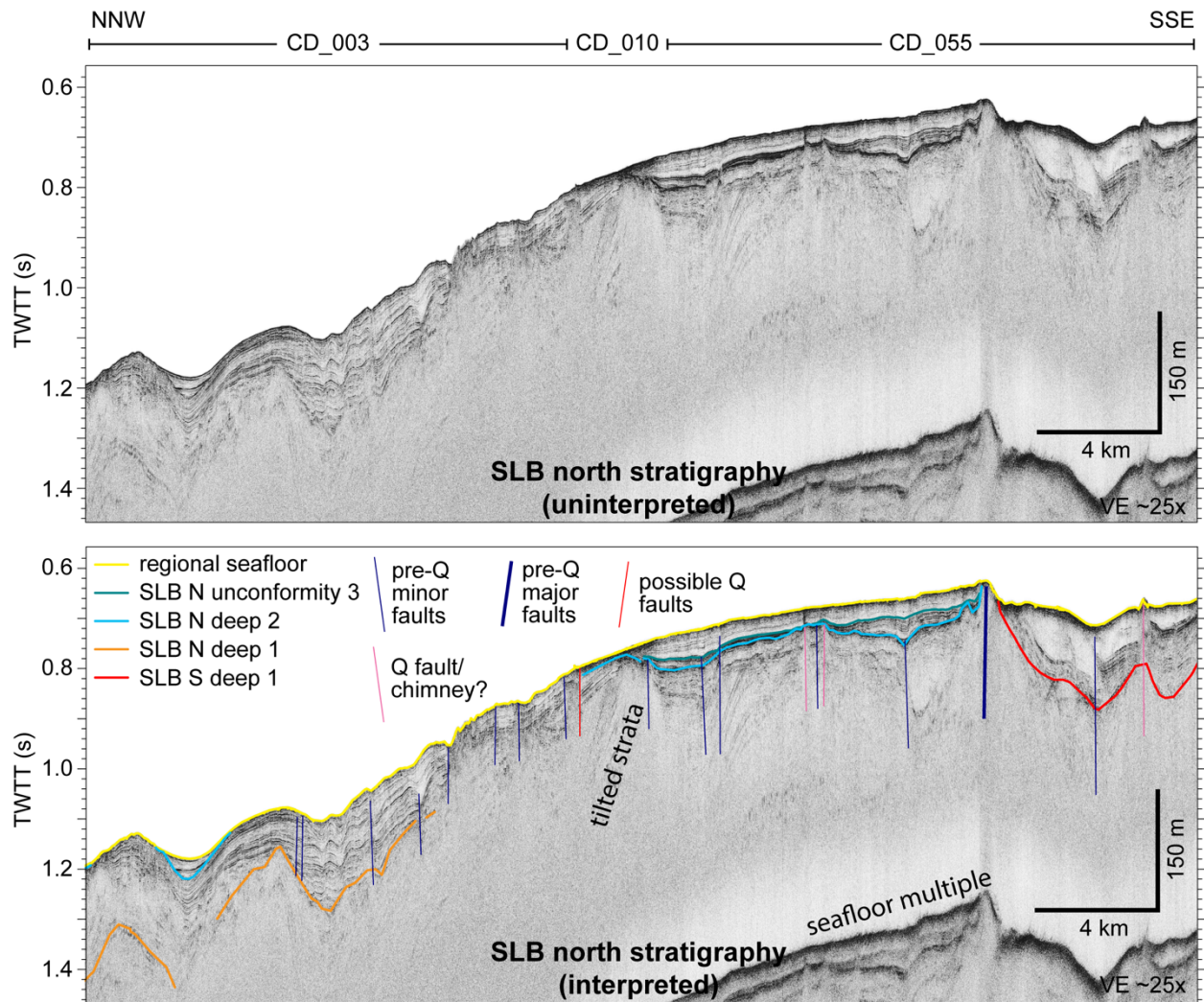


Figure 10. MCS image showing subsurface mapping in the SLB north area.

This multi-channel seismic (MCS) image contains seismic reflection data and interpretations along sections of 3 profiles (labeled at the top of the image as CD_003, CD_010, and CD_055) from the 2018 *Rainier* survey and shows examples of subsurface mapping of horizons located in the SLB north area (line location in Figs. 2 and 9). These horizons were mapped on MCS data throughout the study area and gridded (grids shown in Fig. 9). The MCS data are displayed as envelope traces in two-way travel time (TWTT) with an automatic gain control (AGC) window of 0.5 seconds. Q – Quaternary. Pre-Q – pre-Quaternary. SLB N – Santa Lucia Bank North. SLB S – Santa Lucia Bank South.

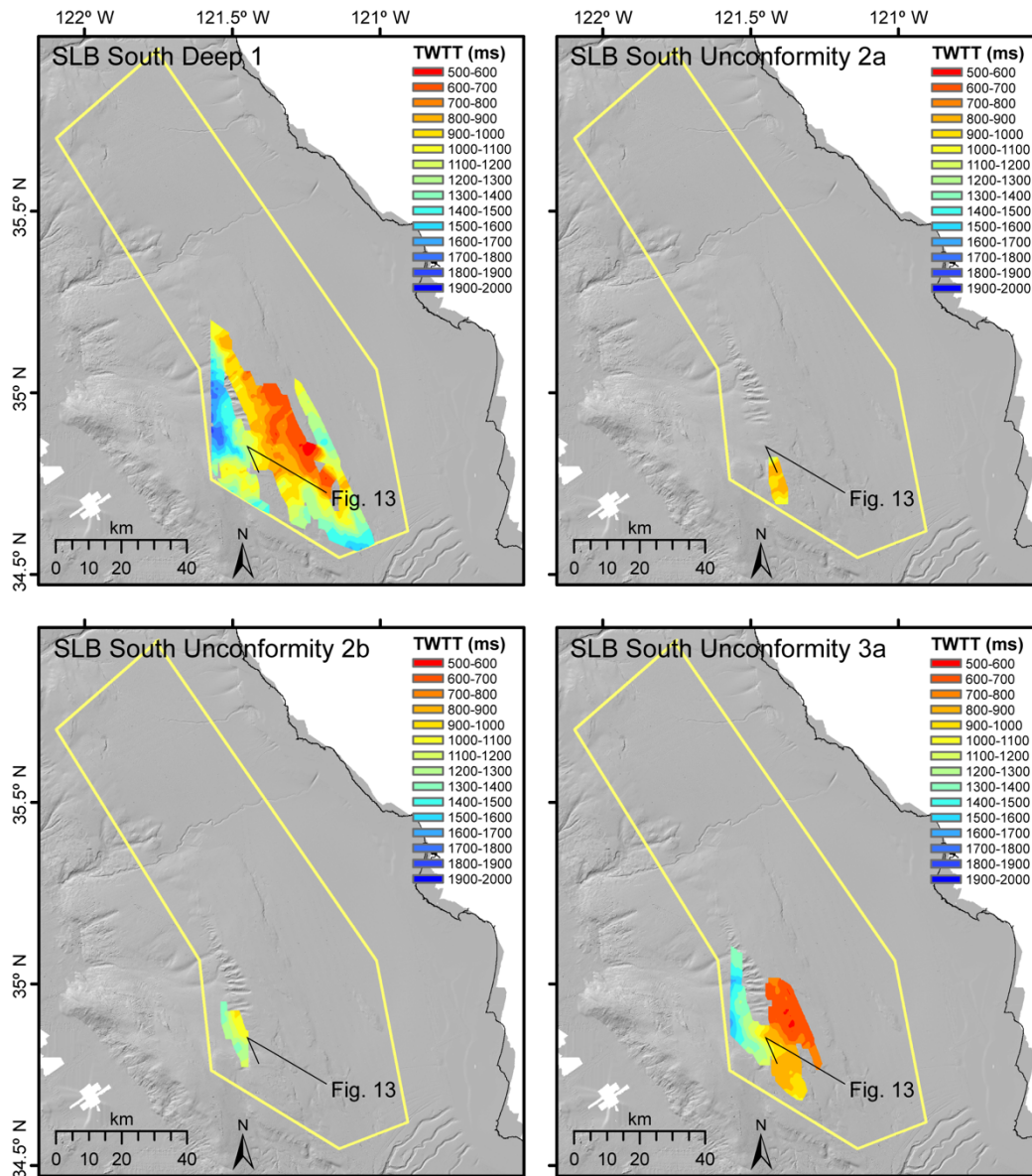


Figure 11. Maps of gridded subsurface horizons in the SLB south area (1 of 2).

Each labeled panel shows a gridded subsurface horizon located within the Santa Lucia Banks (SLB) south physiographic region of the study area. All surfaces display the same color scale to emphasize the relative differences in depth. A labeled black line shows the location of the corresponding seismic crossing in Fig. 13, which has examples of each of the surfaces in the multi-channel seismic (MCS) data (with the exception of the localized SLB South Unconformity 2b). The California Deepwater Investigations and Groundtruthing (Cal DIG) I study area is shown as a yellow outline, and the basemap is a grayscale bathymetric hillshade image from the merged Monterey Bay Aquarium Research Institute (MBARI) bathymetry map shown in Figs. 1, 2, and 3. The spatial extents of each map matches those of Figs. 1, 2, and 3 in order to show the regional coverage of each grid.

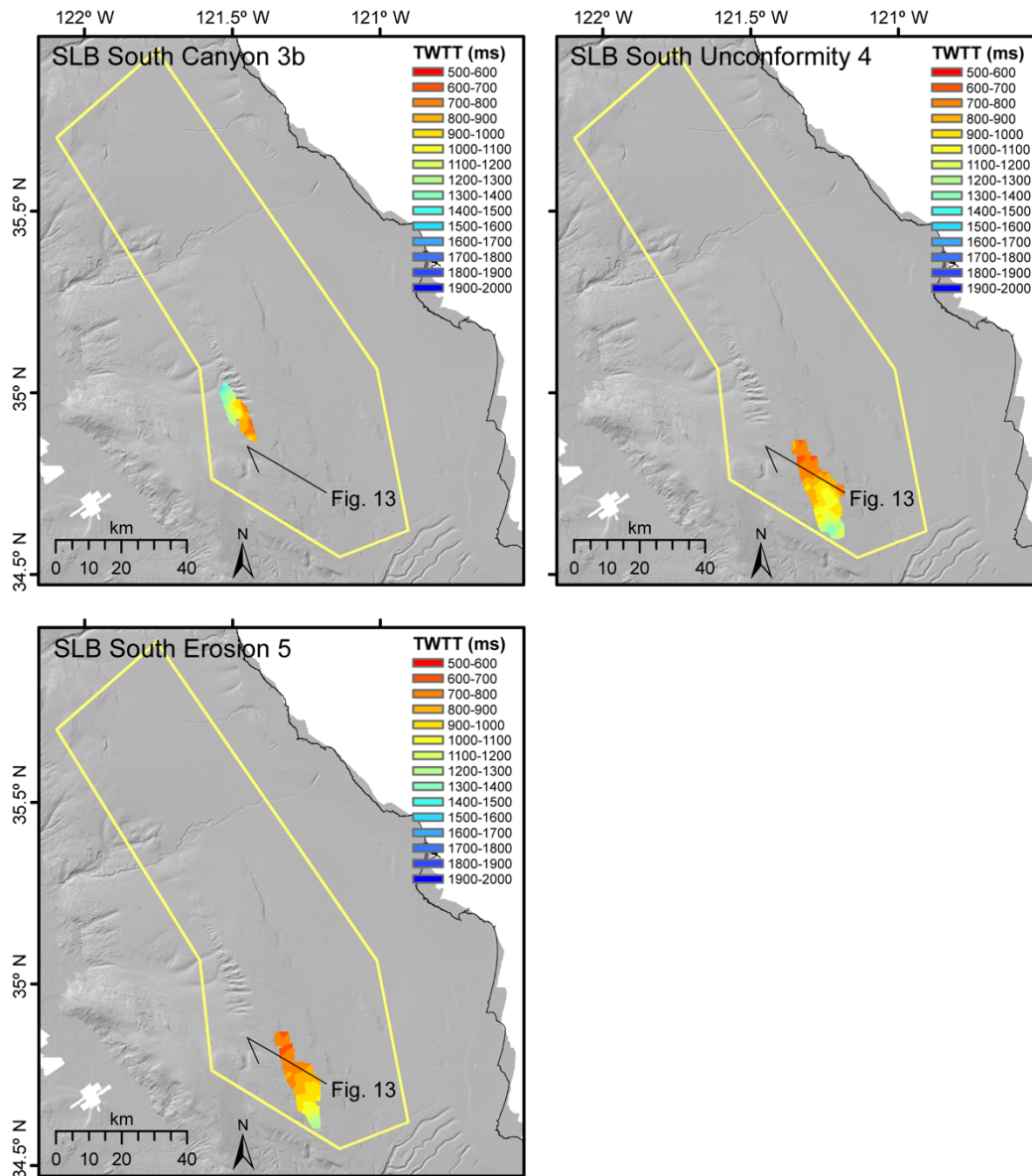


Figure 12. Maps of gridded subsurface horizons in the SLB south area (2 of 2).

Each labeled panel shows a gridded subsurface horizon located within the Santa Lucia Bank (SLB) south physiographic region of the study area. All surfaces display the same color scale (in two-way travel time, TWTT) to emphasize the relative differences in depth. A labeled black line shows the location of the corresponding seismic crossing in Fig. 13, which has examples of each of the surfaces in the multi-channel seismic (MCS) data (with the exception of the localized SLB South Canyon 3b surface). The California Deepwater Investigations and Groundtruthing (Cal DIG) I study area is shown as a yellow outline, and the basemap is a grayscale bathymetric hillshade image from the merged Monterey Bay Aquarium Research Institute (MBARI) bathymetry map shown in Figs. 1, 2, and 3. The spatial extents of each map matches those of Figs. 1, 2, and 3 in order to show the regional coverage of each grid.

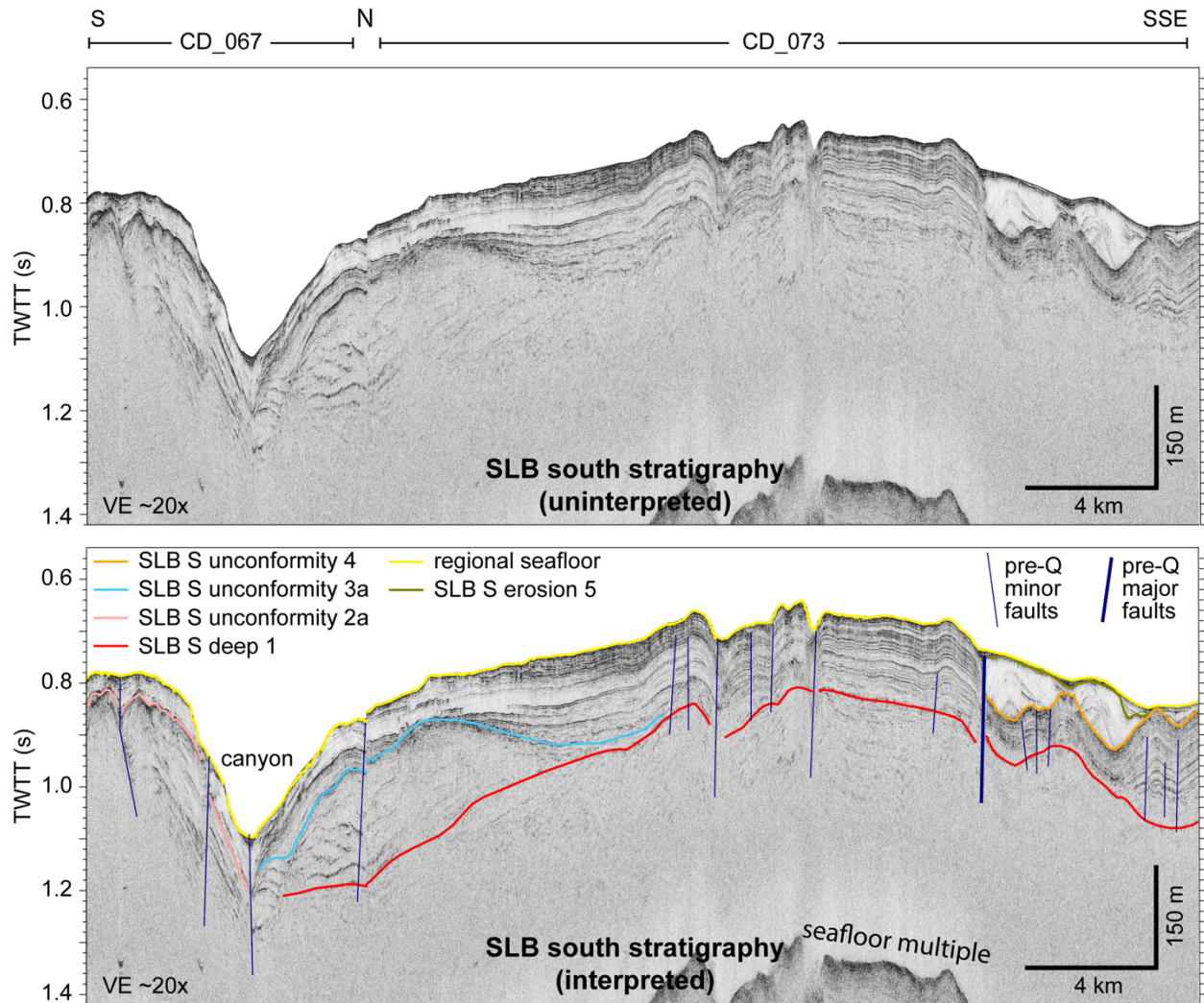
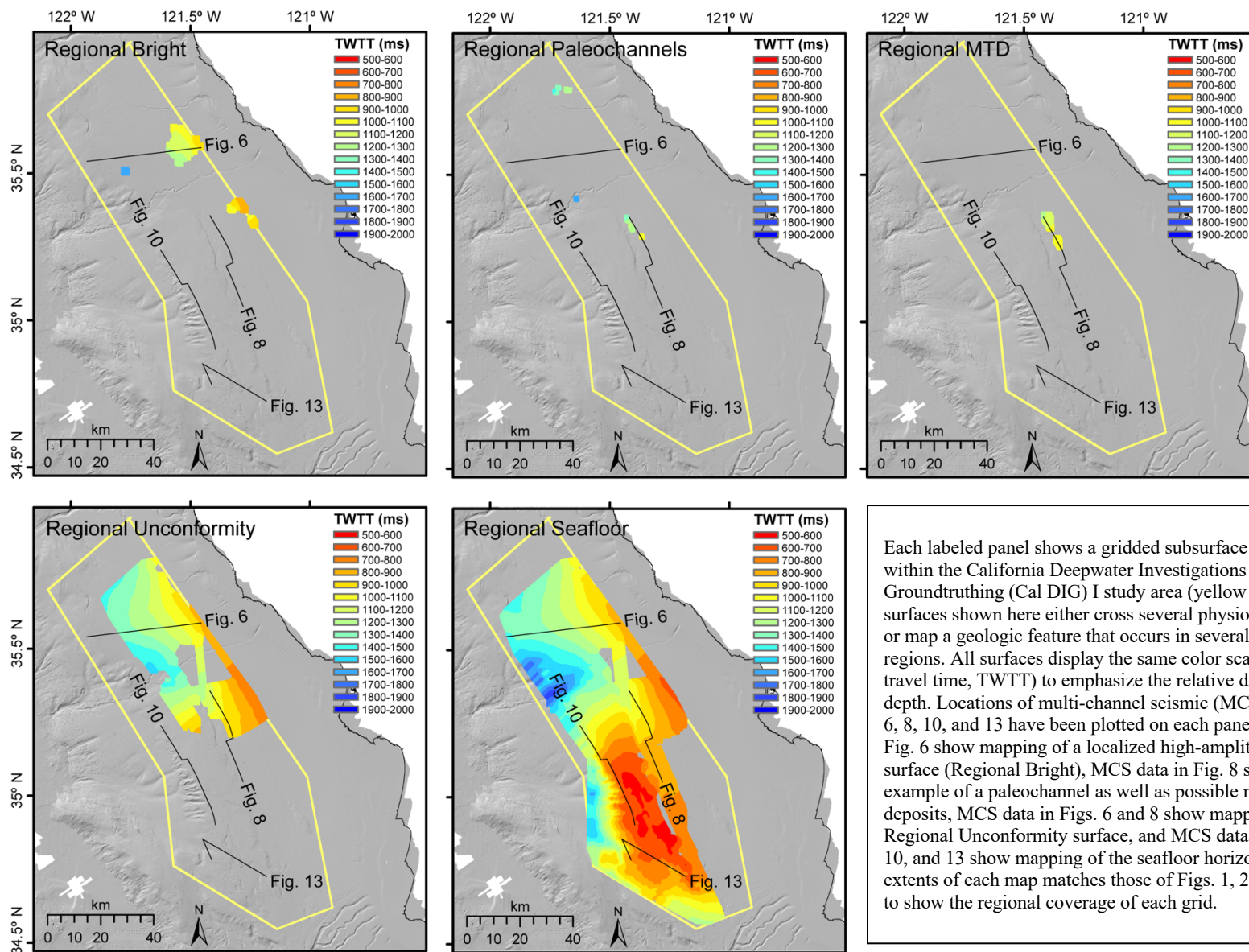


Figure 13. MCS image showing subsurface mapping in the SLB south area.

This multi-channel seismic (MCS) image contains seismic reflection data and interpretations along sections of 2 profiles (labeled at the top of the image as CD_067 and CD_073) from the 2018 *Rainier* survey and shows examples of subsurface mapping of horizons located in the SLB south area (line location in Figs. 2, 11, and 12). These horizons were mapped on MCS data throughout the study area and gridded (grids shown in Figs. 11 and 12). The MCS data are displayed as envelope traces in two-way travel time (TWTT) with an automatic gain control (AGC) window of 0.5 seconds. Pre-Q – pre-Quaternary. SLB S – Santa Lucia Bank South.



Each labeled panel shows a gridded subsurface horizon located within the California Deepwater Investigations and Groundtruthing (Cal DIG) I study area (yellow outline); surfaces shown here either cross several physiographic regions or map a geologic feature that occurs in several physiographic regions. All surfaces display the same color scale (in two-way travel time, TWTT) to emphasize the relative differences in depth. Locations of multi-channel seismic (MCS) data in Figs. 6, 8, 10, and 13 have been plotted on each panel. MCS data in Fig. 6 show mapping of a localized high-amplitude bright surface (Regional Bright), MCS data in Fig. 8 show an example of a paleochannel as well as possible mass-transport deposits, MCS data in Figs. 6 and 8 show mapping of the Regional Unconformity surface, and MCS data in Figs. 6, 8, 10, and 13 show mapping of the seafloor horizon. The spatial extents of each map matches those of Figs. 1, 2, and 3 in order to show the regional coverage of each grid.

Figure 14. Maps of regional gridded subsurface horizons across several physiographic regions.

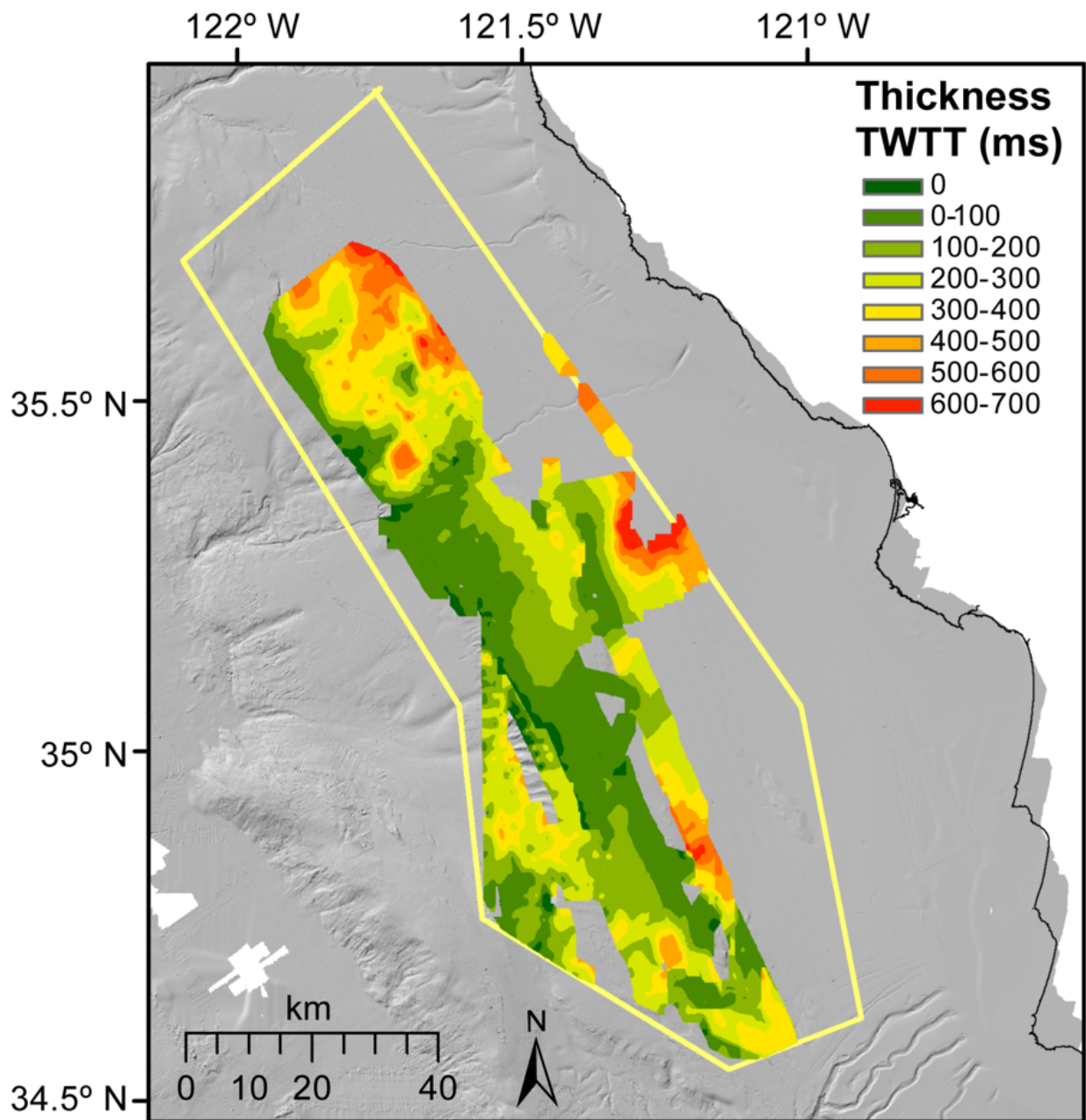


Figure 15. Sediment thickness map.

Map shows difference between the gridded seafloor horizon (Fig. 14) and a merged surface of deep, regionally extensive grids that include basement picks to approximate minimum sediment thickness in the study area (see Methods for details). Note that the color scale is different here than in the other subsurface images but is still shown in two-way travel time (TWTT). Assuming a seismic velocity of 2000 m/s, sediment thickness in TWTT can be loosely approximated as 1 ms = 1 m. A thickness of zero represents little to no sediment cover. The California Deepwater Investigations and Groundtruthing (Cal DIG) I study area is shown as a yellow outline, and the basemap is a grayscale bathymetric hillshade image from the merged Monterey Bay Aquarium Research Institute (MBARI) bathymetry map shown in Figs. 1, 2, and 3. The spatial extents of the map matches those of Figs. 1, 2, and 3.

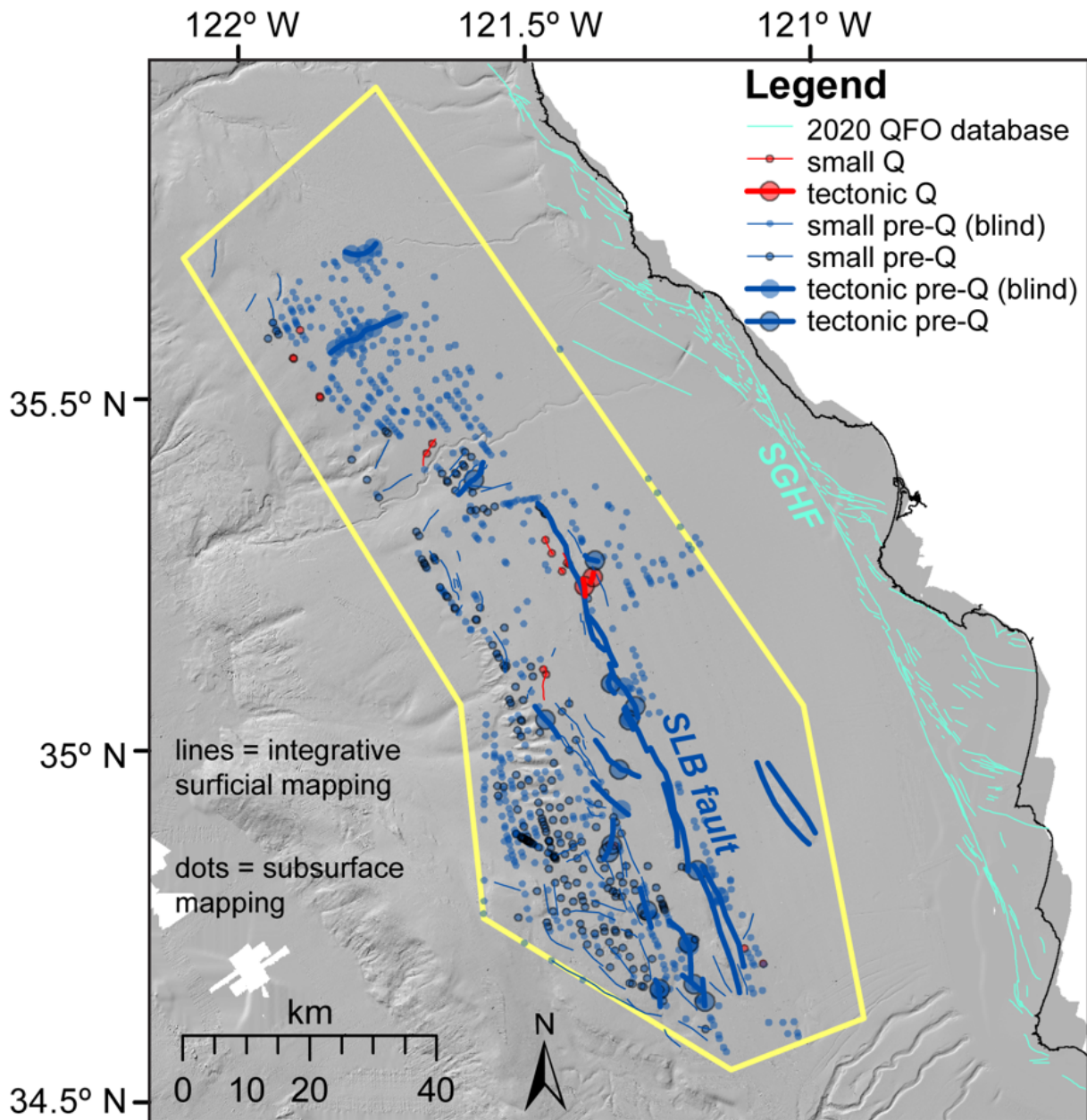


Figure 16. Map of fault structures in the study area.

Map shows surface projections of fault segments identified in the subsurface (points) and continuous faults mapped using integrative bathymetric and subsurface seismic reflection profile interpretations (lines). Points outlined in black indicate fault segments with near-seafloor displacement (mapped displacement within 20 ms two-way travel time (TWTT) of the seafloor), a lack of outline indicates a blind fault. Possibly Quaternary (Q) faults, shown in red, exhibit near-seafloor displacement in sediment interpreted to be Quaternary in age. Mapped pre-Quaternary (pre-Q) faults, shown in blue, displace stratigraphy interpreted to be pre-Quaternary in age. Faults with tectonic offsets are shown as bigger dots and heavier weight lines, whereas smaller-offset structures are shown with smaller dots and thinner lines. Quaternary faults in the USGS Quaternary Faults Offshore of California database (QFO) are shown in light blue near the coastline (see Walton et al., 2020). The California Deepwater Investigations and Groundtruthing (Cal DIG) I study area is shown as a yellow outline, and the basemap is a grayscale bathymetric hillshade image from the merged Monterey Bay Aquarium Research Institute (MBARI) bathymetry map shown in Figs. 1, 2, and 3. The spatial extents of the map matches those of Figs. 1, 2, and 3. SGHF – San Gregorio-Hosgri fault.

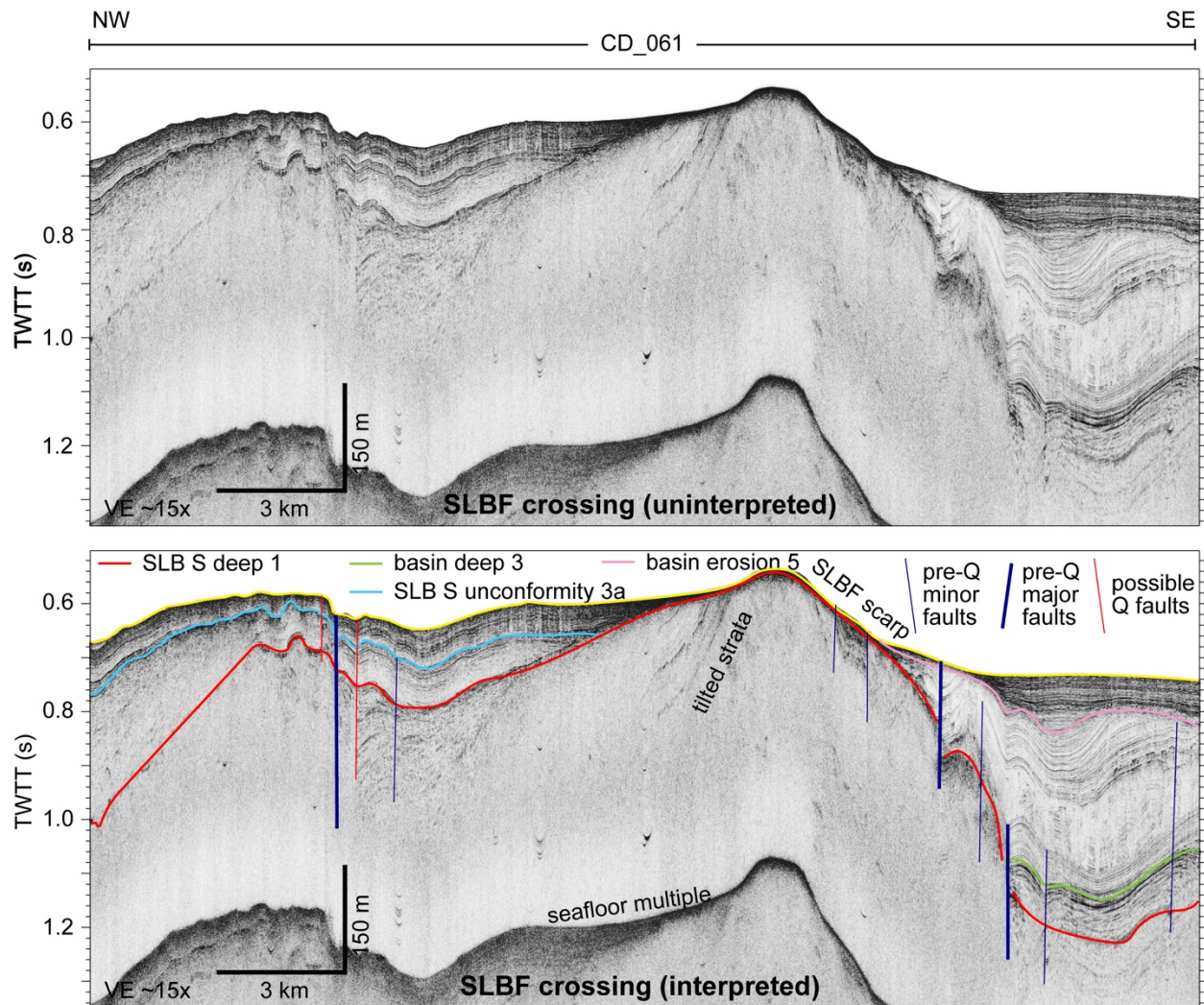


Figure 17. MCS image crossing the Santa Lucia Bank fault.

This multi-channel seismic (MCS) image contains seismic reflection data and interpretations along profile CD_061 from the 2018 *Rainier* survey and is an example of a crossing of the Santa Lucia Bank fault (SLBF). Gridded horizons are shown in Figs. 7 and 11. The MCS data are displayed as envelope traces in two-way travel time (TWTT) with an automatic gain control (AGC) window of 0.5 seconds. Line location is in Fig. 2. SLB S – Santa Lucia Bank South. SLBF – Santa Lucia Bank fault. Pre-Q – pre-Quaternary. Q – Quaternary.

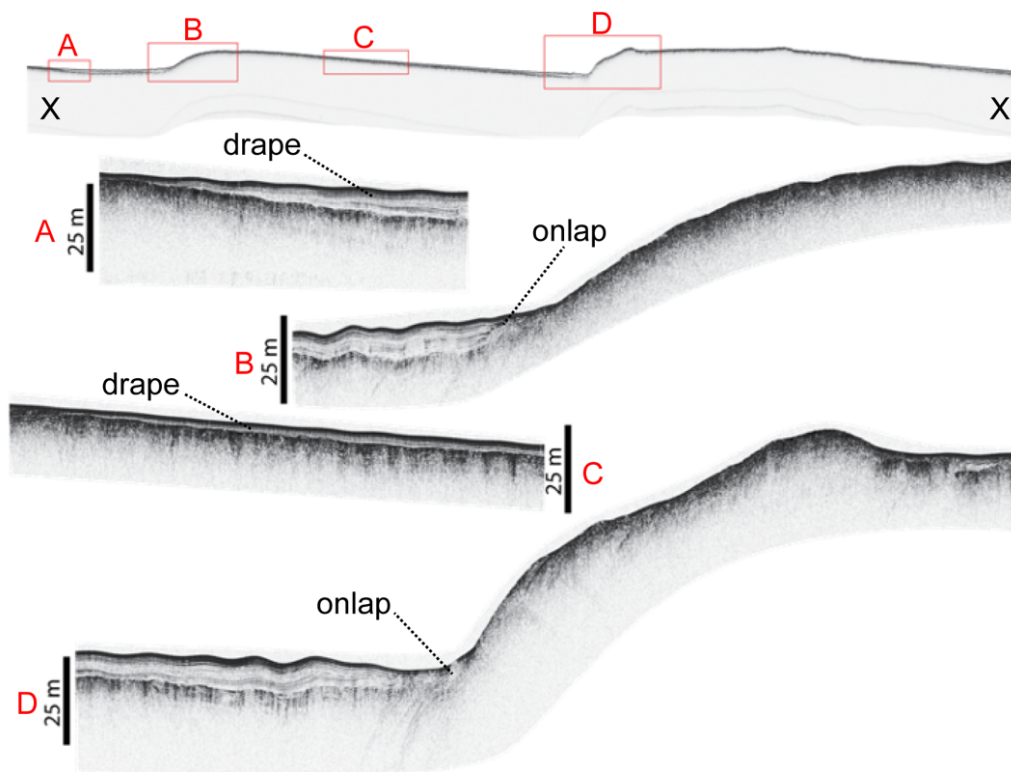
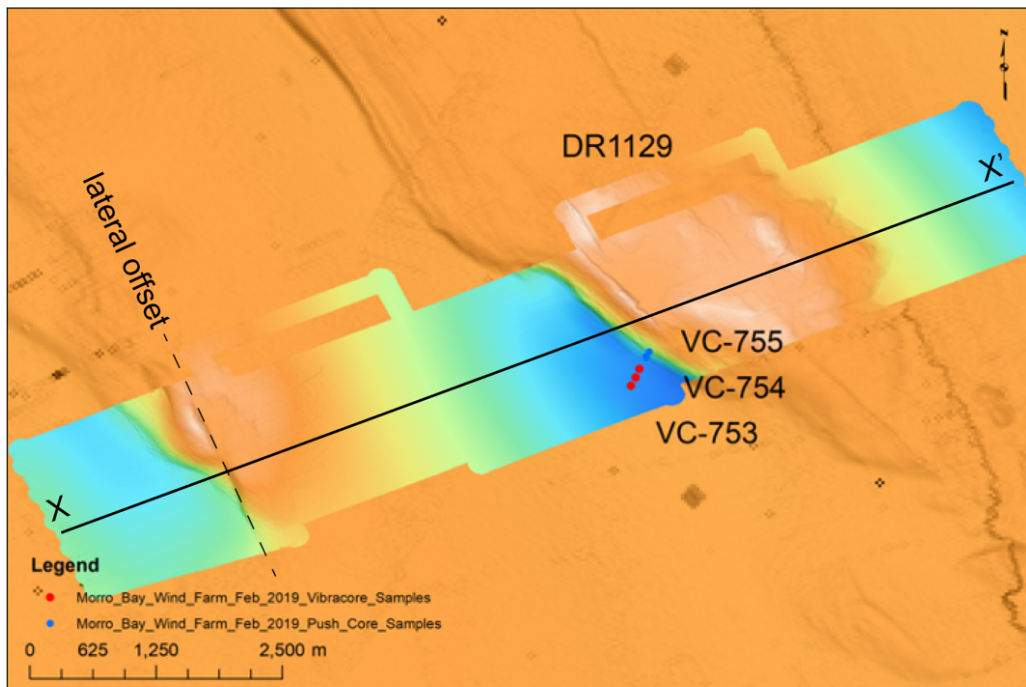


Figure 18. AUV data along SLB scarps.

Top panel shows autonomous underwater vehicle (AUV) bathymetry atop Santa Lucia Bank (SLB) crossing prominent fault scarps (location of AUV survey shown in Fig. 2). Below the bathymetric image, an AUV Chirp sub-bottom profile along profile X-X' is shown. Red boxes A, B, C, and D highlight the locations of four close-ups of the Chirp profile shown at the bottom of the figure.

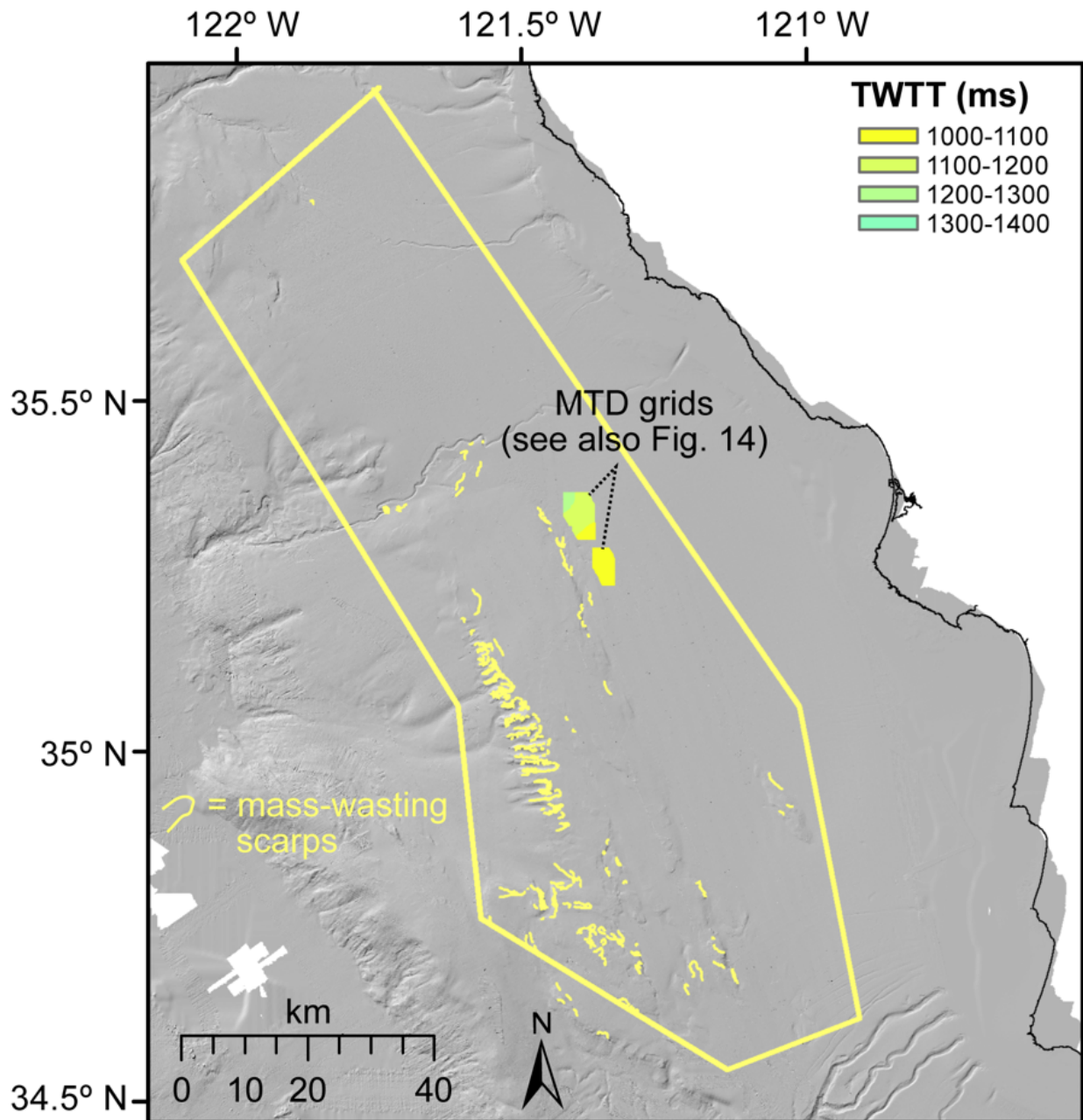


Figure 19. Mapped evidence for mass wasting.

Map shows mapping of scarp-like features on the seafloor that we interpret to be related to mass wasting processes rather than active faulting (yellow lines). Grids of the subsurface mass-transport deposit (MTD) horizons are also shown (see Fig. 14 for another plot of these grids). The California Deepwater Investigations and Groundtruthing (Cal DIG) I study area is shown as a yellow outline, and the basemap is a grayscale bathymetric hillshade image from the merged Monterey Bay Aquarium Research Institute (MBARI) bathymetry map shown in Figs. 1, 2, and 3. The spatial extents of the map matches those of Figs. 1, 2, and 3.

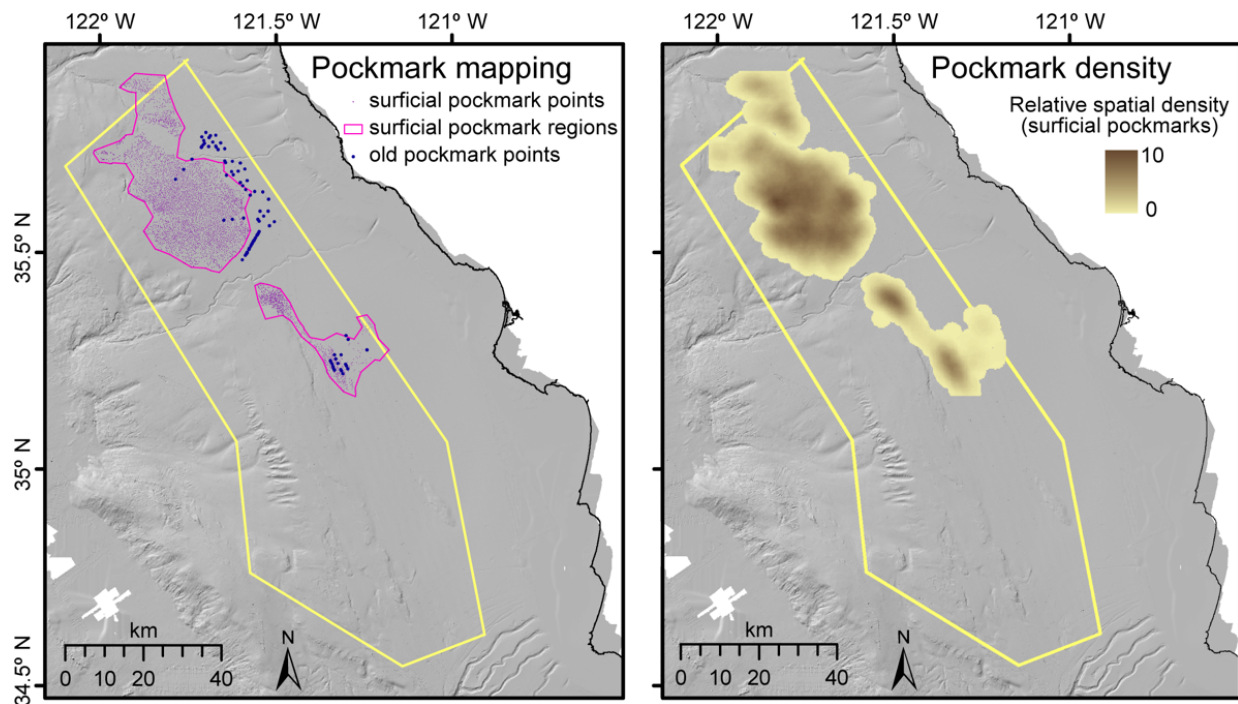


Figure 20. Mapped evidence for pockmarks.

Left map shows hand-digitized surficial pockmark points evident in surface-ship multibeam echosounder (MBES) data (small purple dots) as well as the outlines of the pockmark areas (pink line). Surface projections of buried (old) pockmarks mapped in MCS data are also shown as larger dark blue dots. Examples of buried (old) pockmarks can be seen in the multi-channel seismic (MCS) data shown in Fig. 6. The right map shows a grid of relative density of the modern pockmarks shown in the left map. In both maps, the California Deepwater Investigations and Groundtruthing (Cal DIG) I study area is shown as a yellow outline, and the basemap is a grayscale bathymetric hillshade image from the merged Monterey Bay Aquarium Research Institute (MBARI) bathymetry map shown in Figs. 1, 2, and 3. The spatial extents of each map matches those of Figs. 1, 2, and 3.

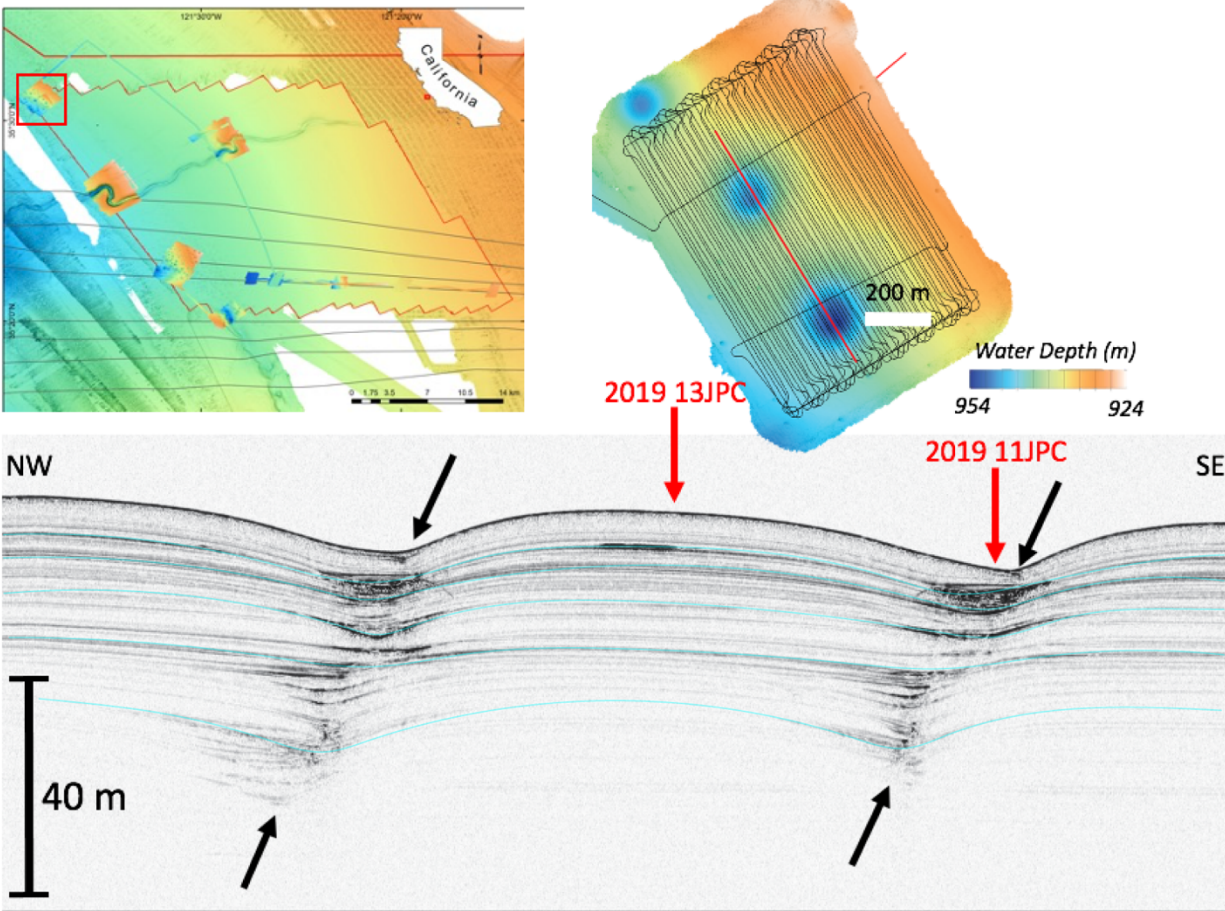


Figure 21. AUV data in the pockmark area.

Top left map shows the approximate location of the autonomous underwater vehicle (AUV) survey (location also called out in the larger map in Fig. 2). Top right image shows an AUV bathymetry survey over several pockmark features. The red line in the upper right image shows the location of the AUV Chirp sub-bottom profile shown at the bottom of the figure, which crosses two of the pockmark features. The black arrows in the Chirp image highlight the drift of the pockmarks over time, and the red arrows show the approximate locations of 2019 R/V *Bold Horizon* piston cores 11JPC and 13JPC. Semi-transparent light blue lines highlight several possible correlative pockmark event horizons.

23JPC Sections 3-5

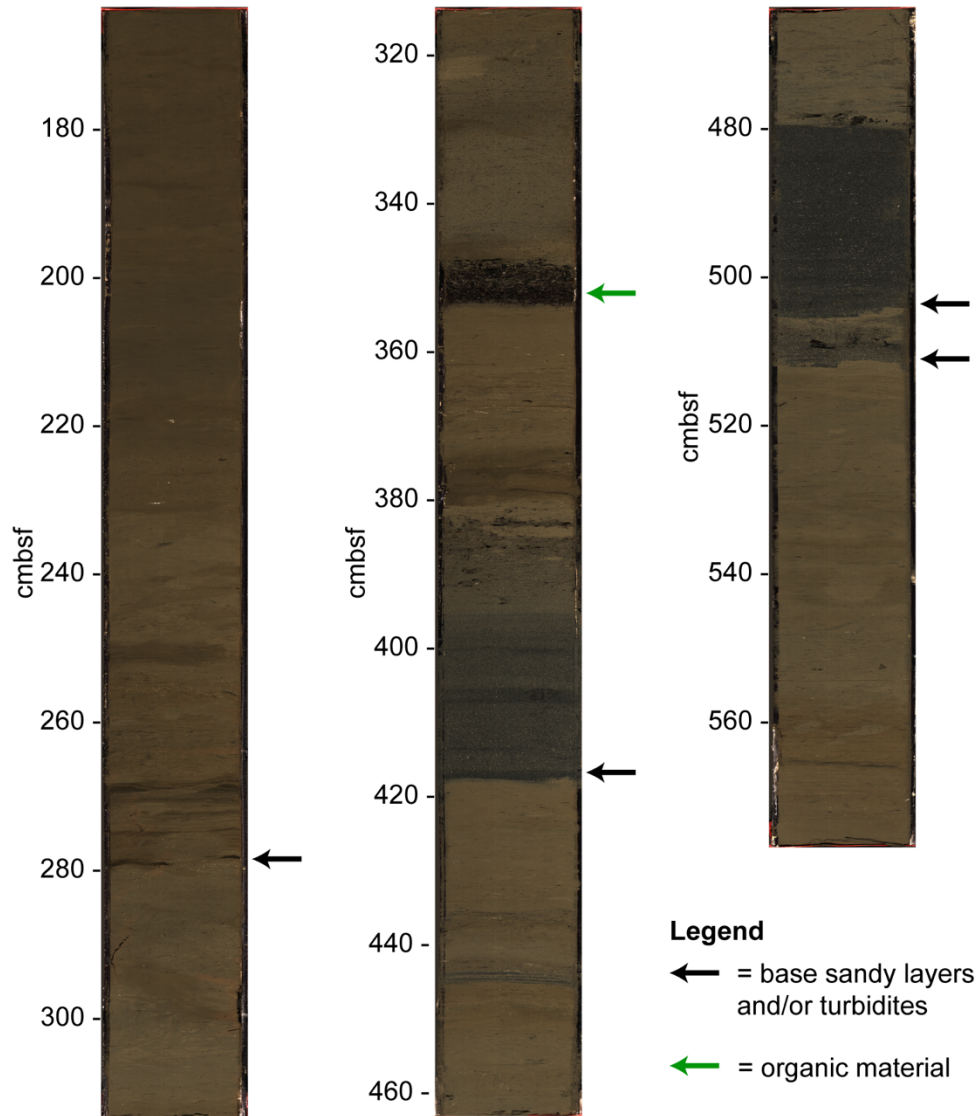


Figure 22. Example piston core photographs from a pockmark core.

Figure shows core photographs from an R/V *Bold Horizon* piston core located in one of the pockmarks, 23JPC sections 3, 4, and 5 from left to right (core location shown in Fig. 3). Arrows highlight sandy turbidite and organic layers. Corresponding computerized tomography (CT) scans of the same sections are shown in Fig. 23, and porewater and multi-sensor core logger (MSCL) data are shown in Fig. 24. Scale values are in cm below seafloor (cmbsf).

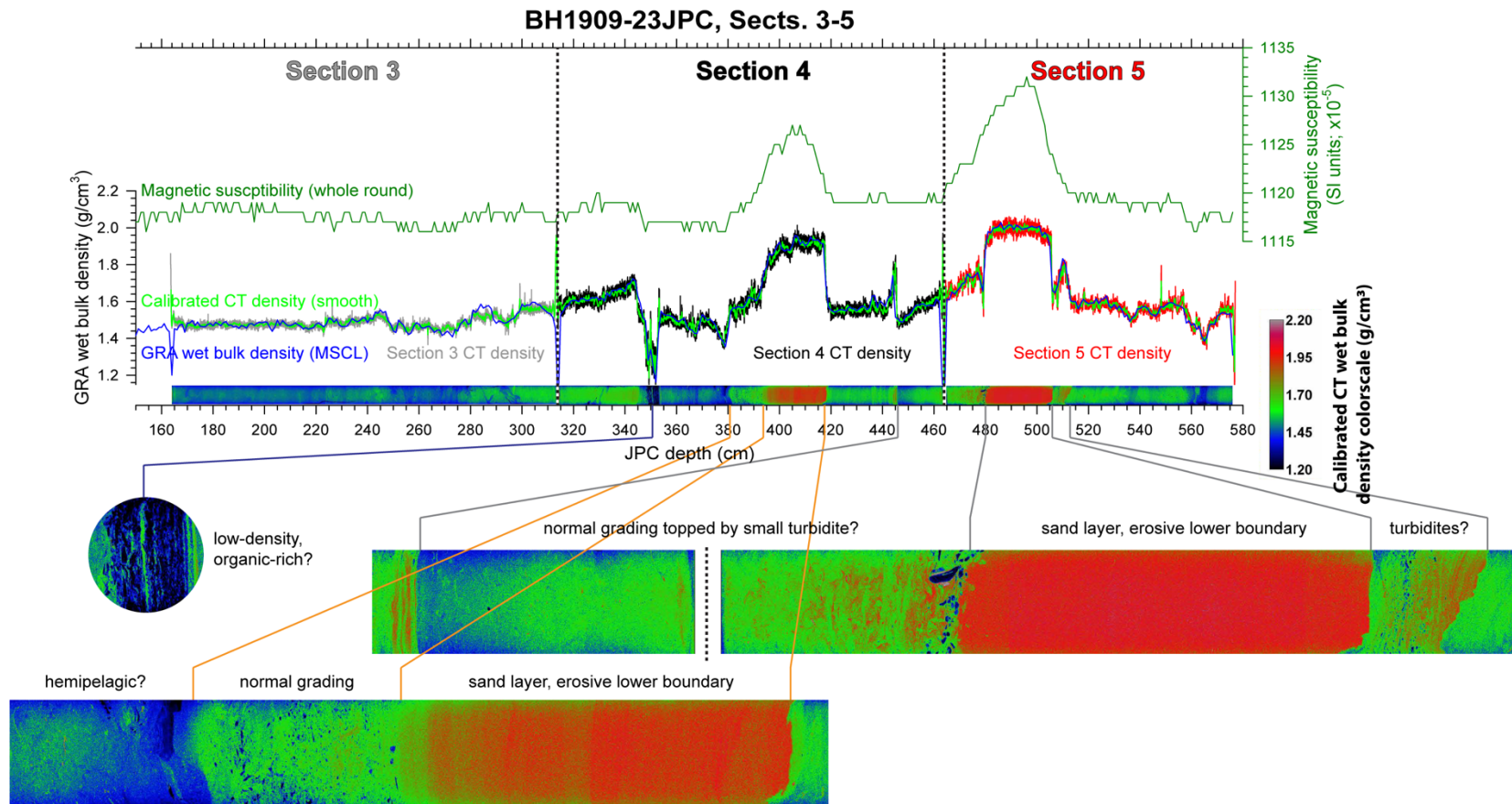


Figure 23. Example CT scan composite plot of a piston core in the pockmark region.

Figure shows computerized tomography (CT) scan data from an R/V *Bold Horizon* piston core located in one of the pockmarks, 23JPC sections 3, 4, and 5 (core location shown in Fig. 3). Insets highlight sandy turbidite and organic layers. Corresponding core photographs of the same sections are shown in Fig. 22, and porewater and multi-sensor core logger (MSCL) data are shown in Fig. 24. Scale values are in cm below seafloor (cmbsf). JPC = jumbo piston core.

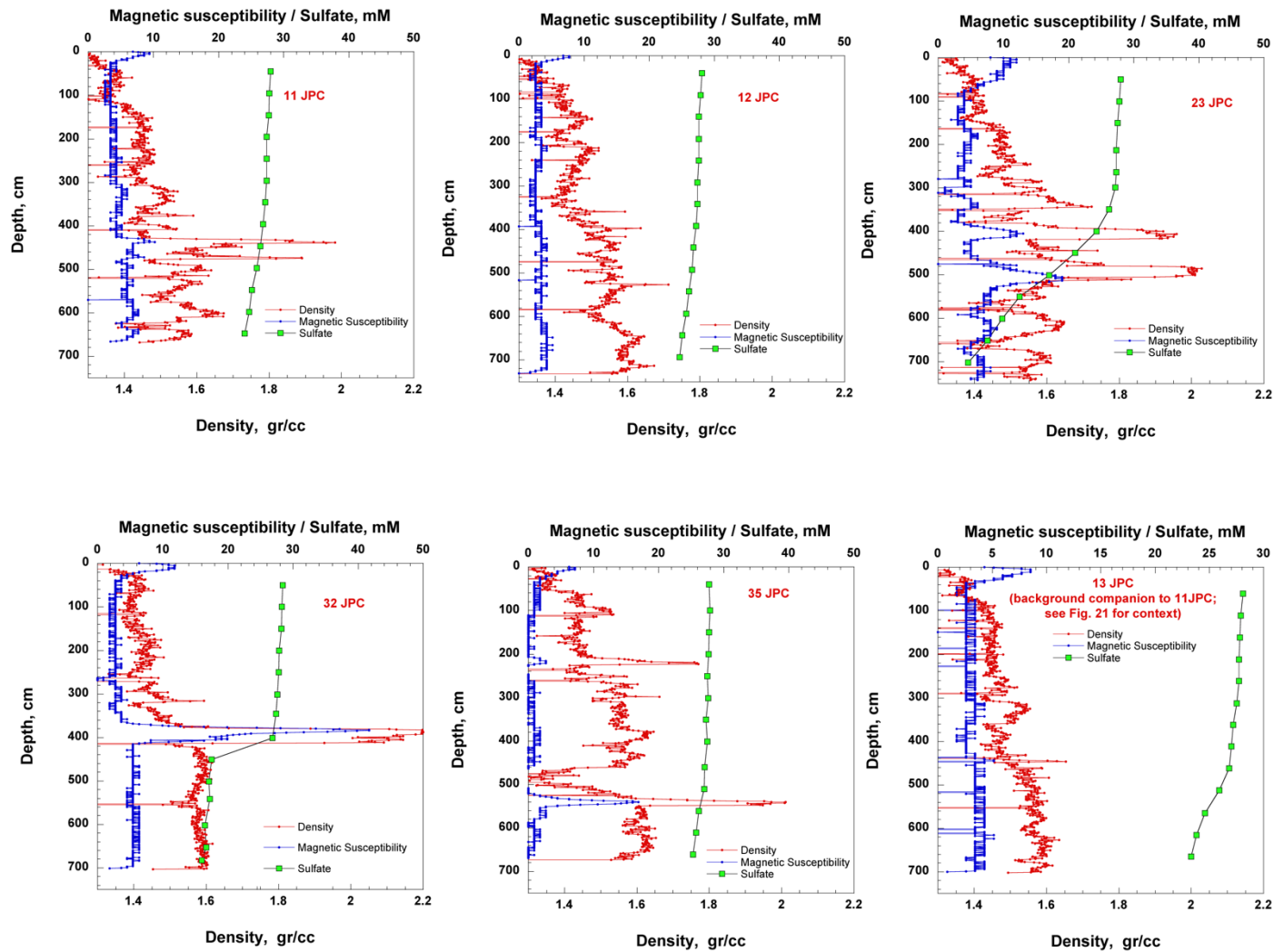


Figure 24. Plot of porewater and MSCL data from pockmark piston cores.

Composite plots of core data from multi-sensor core logger (MSCL) (magnetic susceptibility, density) and porewater (sulfate) analysis for five piston cores from the 2019 R/V Bold Horizon survey located inside pockmarks (11JPC, 12JPC, 23JPC, 32JPC, and 35JPC) and one background core collected just outside of a pockmark for comparison (13JPC, the companion to 11JPC; see Fig. 21 for context and location). The locations of the cores are shown on Fig. 3, 11JPC and 13JPC are also shown on Fig. 21, and core photographs and computerized tomography (CT) scan data from 23JPC is shown in Figs. 22 and 23, respectively.

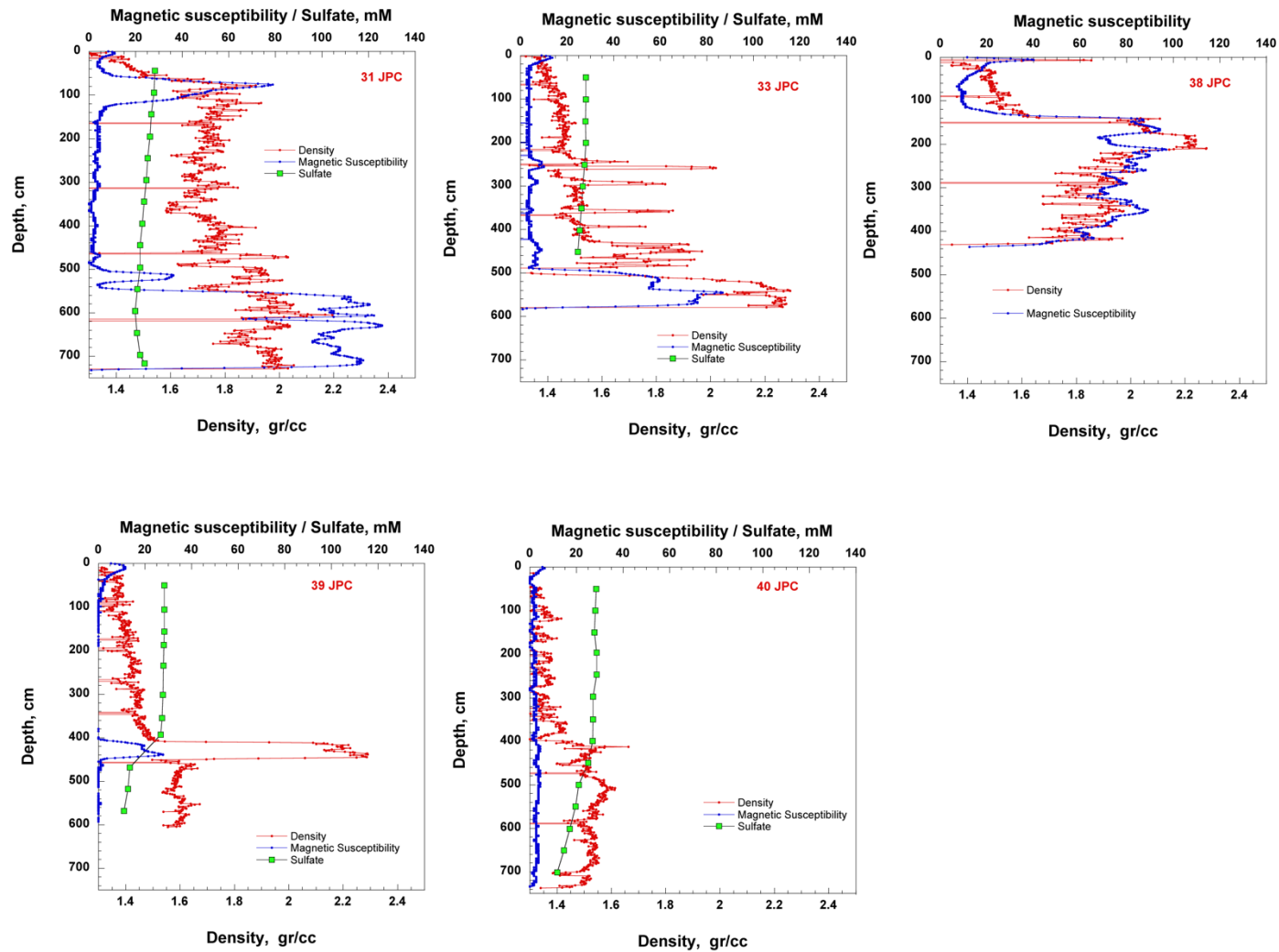


Figure 25. Plot of porewater and MSCL data from the Lucia Chica channel area.

Composite plots of core data from multi-sensor core logger (MSCL) (magnetic susceptibility, density) and porewater (sulfate) analysis for five piston cores from the 2019 R/V Bold Horizon survey located inside pockmarks (11JPC, 12JPC, 23JPC, 32JPC, and 35JPC) and one background core collected just outside of a pockmark for comparison (13JPC, the companion to 11JPC; see Fig. 21 for context and location). The locations of the cores are shown on Fig. 3, 11JPC and 13JPC are also shown on Fig. 21, and core photographs and computerized tomography (CT) scan data from 23JPC is shown in Figs. 22 and 23, respectively.

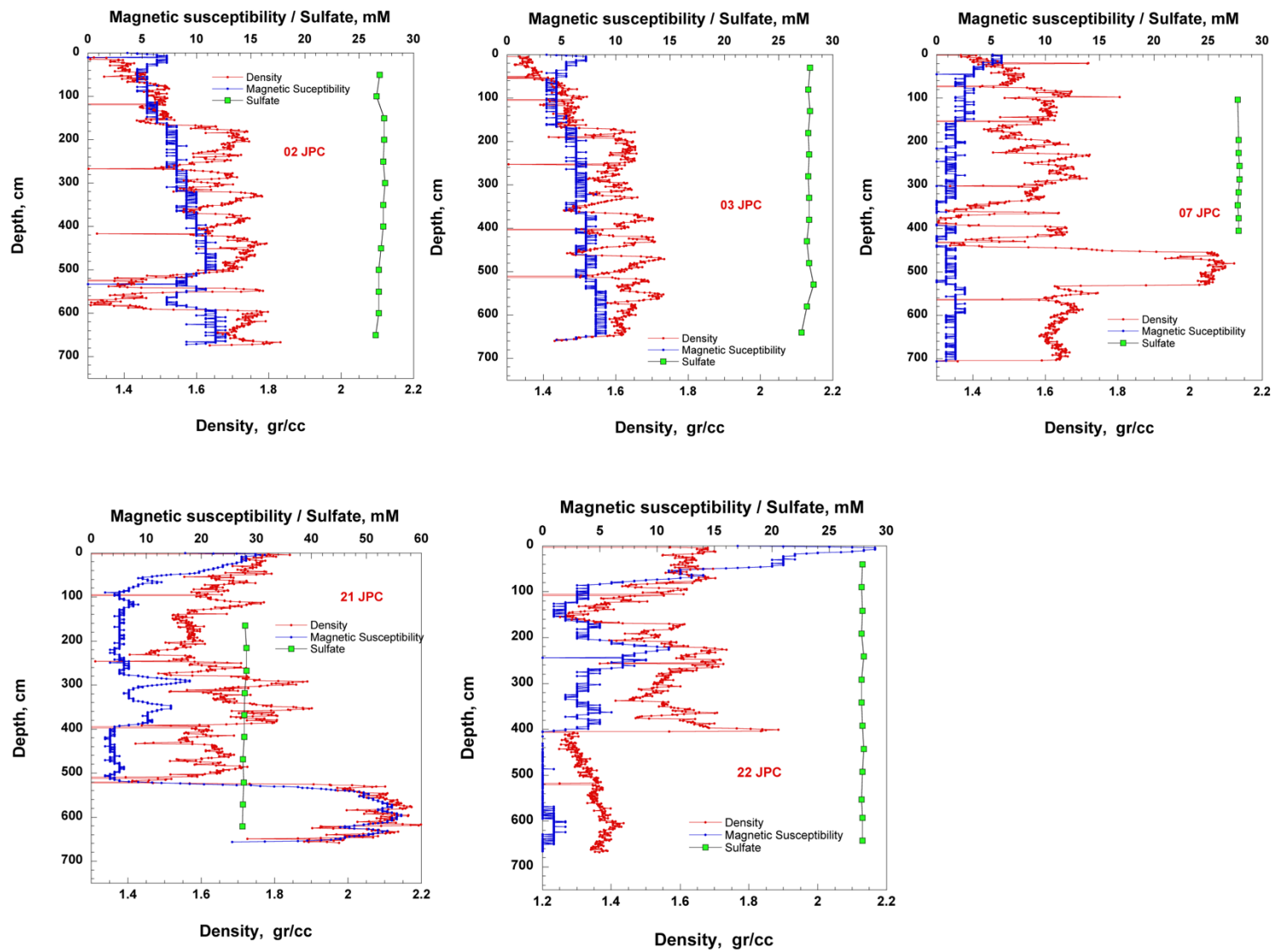


Figure 26. Plot of porewater and MSCL data from piston cores located downslope and east of SLB.

Composite plots of core data from multi-sensor core logger (MSCL) (magnetic susceptibility, density) and porewater (sulfate) analysis for five piston cores from the 2019 R/V Bold Horizon survey located downslope of the eastern edge of SLB (02JPC, 03JPC, 07JPC, 21JPC, and 22JPC). The locations of the cores are shown on Fig. 3.

DR1129 Vibracore Transect

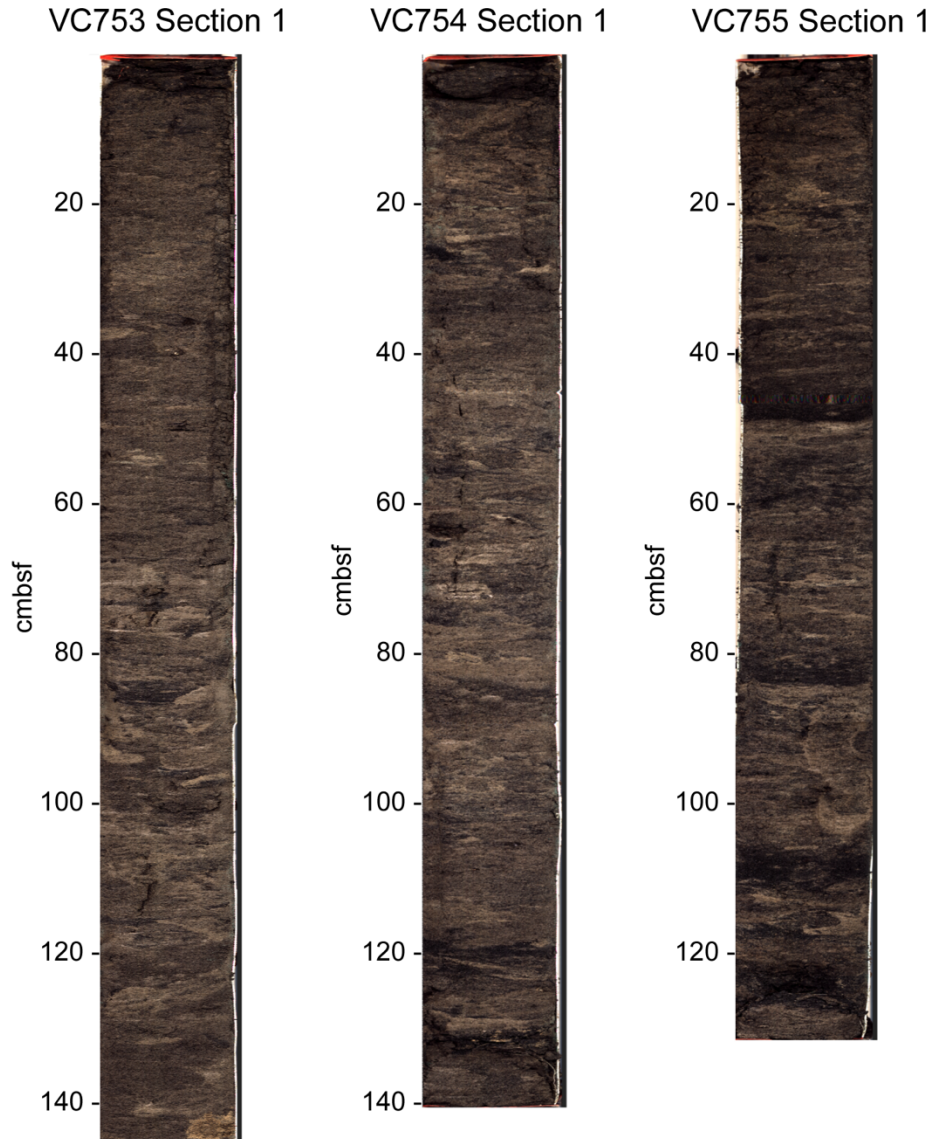


Figure 27. Example vibracore photographs from a transect along an SLB fault.

Figure shows core photograph data from a transect of Monterey Bay Aquarium Research Institute (MBARI) R/V Western Flyer vibracores located along one of the Santa Lucia Bank (SLB) scarps, DR1129 VC753, VC754, and VC755 (location of cores shown on Fig. 18).

6 References

- Borowski WS, Paull CK, Ussler W. 1999. Global and local variations of interstitial sulfate gradients in deep-water, continental margin sediments: Sensitivity to underlying methane and gas hydrates. *Marine Geology* 159(1-4):131-54.
- Bouma A. 1962. *Sedimentology of some Flysch deposits; a graphic approach to facies interpretation*, Published Ph.D. Thesis, Elsevier.
- Bureau of Ocean Energy Management (BOEM). 2018. Commercial Leasing for Wind Power Development on the Outer Continental Shelf (OCS) Offshore California (Call for Information and Nominations). In: Federal Register 83:203 (October 19, 2018) p. 53096. Available from <https://www.boem.gov/california> (Accessed December 2020).
- Caress D, Thomas H, Kirkwood W, McEwen R, Henthorn R, et al. 2008. High-Resolution Multibeam, Sidescan, and Subbottom Surveys Using the MBARI AUV. *Alaska Sea Grant College Program, Univ. of Alaska, Fairbanks*.
- Cochrane G, Kuhn LA, Gilbane L, Paull CK, Walton MAL. 2021a (in prep). California Deepwater Investigations and Groundtruthing (Cal DIG) I, Volume 3: Benthic Habitat Characterization Offshore Morro Bay. *US Geological Survey Open-File Report. Bureau of Ocean Energy Management OCS Study BOEM 2021-045*.
- Cochrane G, Kuhn LA, Gilbane L, Paull CK, Walton MAL. 2021b. Multibeam echo sounder, video observation, and derived benthic habitat data offshore of south-central California in support of the Bureau of Ocean Energy Management Cal DIG, offshore alternative energy project. *U.S. Geological Survey data release*, <https://doi.org/10.5066/P9QQZ27U>.
- Dickens GR, Koelling M, Smith DC, Schnieders L, and the IODP Expedition 302 Scientists. 2007. Rhizon Sampling of Pore Waters on Scientific Drilling Expeditions: An Example from the IODP Expedition 302, Arctic Coring Expedition (ACEX). *Scientific Drilling* 2007 4: 22-25.
- Dickinson WR, Ducea M, Rosenberg LI, Greene HG, Graham SA, Clark JC, Weber GE, Kidder S, Ernst WG, Brabb EE. 2005. Net dextral slip, Neogene San Gregorio–Hosgri fault zone, coastal California: Geologic evidence and tectonic implications. *Geological Society of America Special Paper* 391, 43 pp, doi: 10.1130/2005.2391.
- Dobbs S, Addison JA, Cochrane G, Gwiazda R, Lorenson T, et al. 2020. Submarine waveform field records enhanced frequency of sediment transport events during the Pleistocene, offshore Morro Bay, California. *AGU Fall Meeting 2020*.
- Gawthrop W. 1975. *Seismicity of the central California coastal region. Rep. 2331-1258*, U.S. Geological Survey.
- Gawthrop W. 1978. The 1927 Lompoc, California earthquake. *Bulletin of the Seismological Society of America* 68: 1705-16.
- Goldfinger C, Nelson CH, Morey AE, Johnson JE, Patton JR, et al. 2012. *Turbidite event history—Methods and implications for Holocene paleoseismicity of the Cascadia subduction zone. Rep. 2330-7102*, U.S. Geological Survey.

- Helmberger DV, Somerville PG, Garnero E. 1992. The location and source parameters of the Lompoc, California, earthquake of 4 November 1927. *Bulletin of the Seismological Society of America* 82(4): 1678-1709.
- Holbrook W, Gorman A, Hornbach M, Hackwith K, Nealon J, et al. 2002. Seismic detection of marine methane hydrate. *The Leading Edge* 21: 686-9.
- Johnson SY, Watt JT, Hartwell SR, Kluesner JW. 2018. Neotectonics of the Big Sur Bend, San Gregorio-Hosgri Fault System, Central California. *Tectonics* 37: 1930-54.
- Kennedy DJ, Walton MAL, Cochran GR, Balster-gee AF, Kluesner JW, Hart PE, Sliter RW, Miller JK, Gilbane L. 2021a. High-resolution multi-channel and Chirp seismic-reflection data from USGS cruise 2018-641-FA collected in south-central California in support of the Bureau of Ocean Energy Management Cal DIG I offshore alternative energy project. *U.S. Geological Survey data release*, <https://doi.org/10.5066/P9JU17GE>.
- Kennedy DJ, Walton MAL, Cochran GR, Paull CK, Caress DW, Anderson K, and Lundsten E. 2021b. Donated AUV bathymetry and Chirp data collected during Monterey Bay Aquarium Research Institute cruises in 2018-2019 offshore of south-central California. *U.S. Geological Survey data release*, <https://doi.org/10.5066/P97QM7NF>.
- Kennedy DJ, Walton MAL, Cochran GR, Addison J, Paull CK, Gwiazda R, Lorenson T, and Lundsten E. 2021c. Piston and gravity core data collected during USGS cruise 2019-642-FA offshore of south-central California in support of the Bureau of Ocean Energy Management Cal DIG I offshore alternative energy project. *U.S. Geological Survey data release*, <https://doi.org/10.5066/P9DE639J>.
- Kennedy DJ, Walton MAL, Cochran GR, Paull CK, Gwiazda R, Kuhn L, Lundsten E, Addison J, Lorenson T, McGann M, Nieminski N. 2021d. Donated ROV vibracore and sampling data collected during Monterey Bay Aquarium Research Institute cruises in 2019 offshore of south-central California. *U.S. Geological Survey data release*, <https://doi.org/10.5066/P9E2OP35>.
- Kuhn L, Gilbane L, Cochran G, Paull CK. 2021. California Deepwater Investigations and Groundtruthing (Cal DIG) I, Volume 1: Biological Site Characterization Offshore Morro Bay. Camarillo (CA): US Department of the Interior, Bureau of Ocean Energy Management. OCS Study BOEM 2021-037. 72 p.
- Lundsten E, Paull C, Caress DW, Gwiazda R, Cochran G, et al. 2019. Commingled Seafloor Pockmarks and Micro Depressions Offshore Big Sur, California. *AGU Fall Meeting 2019*.
- Maier KL, Fildani A, McHargue TR, Paull CK, Graham SA, Caress DW. 2012. Punctuated Deep-Water Channel Migration: High-Resolution Subsurface Data from the Lucia Chica Channel System, Offshore California, USA. *Journal of Sedimentary Research* 82: 1-8.
- Maier KL, Fildani A, Paull CK, Graham SA, McHargue TR, et al. 2011. The elusive character of discontinuous deep-water channels: New insights from Lucia Chica channel system, offshore California. *Geology* 39: 327-30.
- Maier KL, Fildani A, Paull CK, McHargue TR, Graham SA, Caress DW. 2013. Deep-sea channel evolution and stratigraphic architecture from inception to abandonment from high-resolution Autonomous Underwater Vehicle surveys offshore central California. *Sedimentology* 60: 935-60.

- Mazzini A, Svensen HH, Forsberg CF, Linge H, Lauritzen S-E, et al. 2017. A climatic trigger for the giant Troll pockmark field in the northern North Sea. *Earth and Planetary Science Letters* 464: 24-34.
- McCulloch DS. 1987. Regional geology and hydrocarbon potential of offshore central California.
- McCulloch DS, Clarke S, Dolton G, Field M, Scott E, Utter P. 1982. Geology, environmental hazards, and petroleum resources for 1982 OCS lease sale 73, offshore central and northern California. *U.S. Geological Survey Open-File Report 82-1000*.
- McCulloch DS, Greene H, Heston K, Rubin D. 1980. A Summary of the Geology and Geological Hazards in Proposed Lease Sale 53, Central California Outer Continental Shelf. *U.S. Geological Survey Open-File Report 80-1095*.
- Namson J, Davis TL. 1990. Late Cenozoic Fold and Thrust Belt of the Southern Coast Ranges and Santa Maria Basin, California. *AAPG Bulletin* 74: 467-92.
- Normark WR, Gutmacher CE. 1988. Sur submarine slide, Monterey fan, central California. *Sedimentology* 35: 629-47.
- Paull C, Ussler III W, Maher N, Greene HG, Rehder G, Lorenson T, Lee H. 2002. Pockmarks off Big Sur, California. *Marine Geology* 181: 323-35. doi:[https://doi.org/10.1016/S0025-3227\(01\)00247-X](https://doi.org/10.1016/S0025-3227(01)00247-X).
- Reeburgh WS, 1980. Anaerobic methane oxidation: rate and depth distribution in Skan Bay marine sediments. *Earth and Planetary Sciences Letters* 47: 345–352.
- Satake K, Somerville PG. 1992. Location and size of the 1927 Lompoc, California, earthquake from tsunami data. *Bulletin of the Seismological Society of America* 82(4): 1710-1725.
- Walton MAL, Papesh AG, Johnson SY, Conrad JE, Brothers DS. 2020. Quaternary faults offshore of California. *U.S. Geological Survey data release*, <https://doi.org/10.5066/P91RYEZ4>.



Department of the Interior (DOI)

The Department of the Interior protects and manages the Nation's natural resources and cultural heritage; provides scientific and other information about those resources; and honors the Nation's trust responsibilities or special commitments to American Indians, Alaska Natives, and affiliated island communities.



Bureau of Ocean Energy Management (BOEM)

The mission of the Bureau of Ocean Energy Management is to manage development of U.S. Outer Continental Shelf energy and mineral resources in an environmentally and economically responsible way.

BOEM Environmental Studies Program

The mission of the Environmental Studies Program is to provide the information needed to predict, assess, and manage impacts from offshore energy and marine mineral exploration, development, and production activities on human, marine, and coastal environments. The proposal, selection, research, review, collaboration, production, and dissemination of each of BOEM's Environmental Studies follows the DOI Code of Scientific and Scholarly Conduct, in support of a culture of scientific and professional integrity, as set out in the DOI Departmental Manual (305 DM 3).